frontiers in Earth Science

ORIGINAL RESEARCH
published: 01 July 2021
doi: 10.3389/feart.2021.668445

Lake-Level Changes and Their Paleo-Climatic Implications at the MIS12 Lower Paleolithic (Middle Pleistocene) Site Marathousa 1, Greece

Ines J. E. Bludau[1,2], Penelope Papadopoulou[3], George Iliopoulos[3], Max Weiss[1], Ellen Schnabel[1], Nicholas Thompson[1,4], Vangelis Tourloukis[1,4], Charlotte Zachow[1], Styliani Kyrikou[1,4], George E. Konidaris[1,4], Panagiotis Karkanas[5], Eleni Panagopoulou[6], Katerina Harvati[1,2,4] and Annett Junginger[1,2]**

[1]Department of Geosciences, Eberhard Karls University Tuebingen, Tuebingen, Germany, [2]Senckenberg Centre for Human Evolution and Palaeoenvironment (S-HEP), Tuebingen, Germany, [3]Department of Geology, University of Patras, Rio Patras, Greece, [4]Paleoanthropology, Institute for Archaeological Sciences, Eberhard Karls University of Tübingen, Tübingen, Germany, [5]The Malcolm H. Wiener Laboratory for Archaeological Science, American School of Classical Studies at Athens, Athens, Greece, [6]Ephoreia of Paleoanthropology-Speleology of Greece, Athens, Greece

OPEN ACCESS

Edited by:
Matthias Prange,
University of Bremen, Germany

Reviewed by:
Li Wu,
Anhui Normal University, China
Steffen Mischke,
University of Iceland, Iceland

***Correspondence:**
Annett Junginger
annett.junginger@uni-tuebingen.de
Ines J. E. Bludau
bludau.ines@gmail.com

Specialty section:
This article was submitted to Quaternary Science, Geomorphology and Paleoenvironment, a section of the journal Frontiers in Earth Science

Received: 16 February 2021
Accepted: 18 May 2021
Published: 01 July 2021

Citation:
Bludau IJ E, Papadopoulou P, Iliopoulos G, Weiss M, Schnabel E, Thompson N, Tourloukis V, Zachow C, Kyrikou S, Konidaris GE, Karkanas P, Panagopoulou E, Harvati K and Junginger A (2021) Lake-Level Changes and Their Paleo-Climatic Implications at the MIS12 Lower Paleolithic (Middle Pleistocene) Site Marathousa 1, Greece. Front. Earth Sci. 9:668445. doi: 10.3389/feart.2021.668445

Lithics and cut-marked mammal bones, excavated from the paleo-lake Marathousa 1 (MAR-1) sediments in the Megalopolis Basin, southern Greece, indicate traces of hominin activity occurring along a paleo-shoreline ca. 444,000 years (444 ka) ago. However, the local environment and climatic conditions promoting hominin activity in the area during the MIS12 glacial remain largely unknown. In order to reconstruct the paleo-environment including paleo-lake levels and governing paleo-climatic factors on a high temporal resolution, we analyzed a 6-meter-long sediment sequence from the archeological site MAR-1 and a Bayesian age model was computed for a better age constrain of the different sedimentary units. A multiproxy approach was applied using ostracods, sponge spicules, diatoms, grain sizes, total organic carbon, total inorganic carbon and conventional X-ray fluorescence analysis. The results from the site represent a protected region surrounded by high mountains under the constant influence of water, either as a shallow partly anoxic water body surrounded by reed belts (>463–457 ka, <434–427 ka), a riverine-lake deltaic system (~457–448 ka), a floodplain (~448–444 ka) or a seasonal freshwater pond (~444–436 ka). The local changes of water levels resemble large trends and rhythms of regional records from the Mediterranean and appear to directly respond to sea surface temperature (SST) changes of the North Atlantic. In particular, when the SSTs are high, more moisture reaches the study area and vice versa. Additional water reaches MAR-1 through melting of the surrounding glaciers after brief warm phases during MIS12 in the Mediterranean realm, which leads to the formation of smaller fresh water ponds, where also the horizon of the excavated remains is placed. Such ponds, rich in ostracods and other microorganisms, provided mammals and humans valuable resources, such as potable water, a wide range of plant species and hunting opportunities. These deposits therefore bear a high archeological potential. The results from our study suggest that the Megalopolis Basin could have served as a refugium for hominins and other organisms due to its capacity to retain freshwater bodies during glacial and interglacial periods.

Keywords: Megalopolis, lignite, XRF, Mediterranean, paleo-lakes, ostracods

INTRODUCTION

Present-day Greece is often proposed to have played a key role in hominin dispersal due to its central geographic position between Africa, Asia and Europe (Harvati et al., 2009; Tourloukis and Karkanas, 2012; Harvati, 2016; Harvati, 2021; Papoulia, 2017; Tourloukis and Harvati, 2018; Harvati et al., 2019). However, there is a conspicuous lack of paleoanthropological/paleolithic remains from this region, with remains assigned to the Lower Paleolithic being especially rare (e.g., Harvati et al., 2009; Tourloukis and Karkanas, 2012; Harvati, 2016; Harvati, 2021; Tourloukis and Harvati, 2018). Several hypotheses have been proposed to account for this scarcity of evidence from Greece (e.g., research bias, loss of sites to rising sea levels, geological factors; see Tourloukis, 2016). The environmental conditions that may have allowed or prevented hominin dispersal and long-term survival in this region, therefore, are of particular interest. Currently, only four sites in Greece can be assigned to the Lower Paleolithic: 1) Kokkinopilos (Epirus), 2) Plakias (Crete), 3) Rodafnidia (Lesvos) and 4) Marathousa 1 (MAR-1; Megalopolis, Peloponnese) (**Figure 1**). Of these, only the Megalopolis Pleistocene sediments present a high potential for paleoenvironmental reconstructions (see, e.g., Harvati et al., 2018 and references therein).

Paleoenvironmental reconstruction from terrestrial archives, such as those from the Marathousa paleo-lake close to the archeological site MAR-1, is a powerful tool to better constrain the local living conditions of the preserved biota. The Marathousa Member (Choremi Formation) sedimentary sequence in the Megalopolis Basin consists of alternating

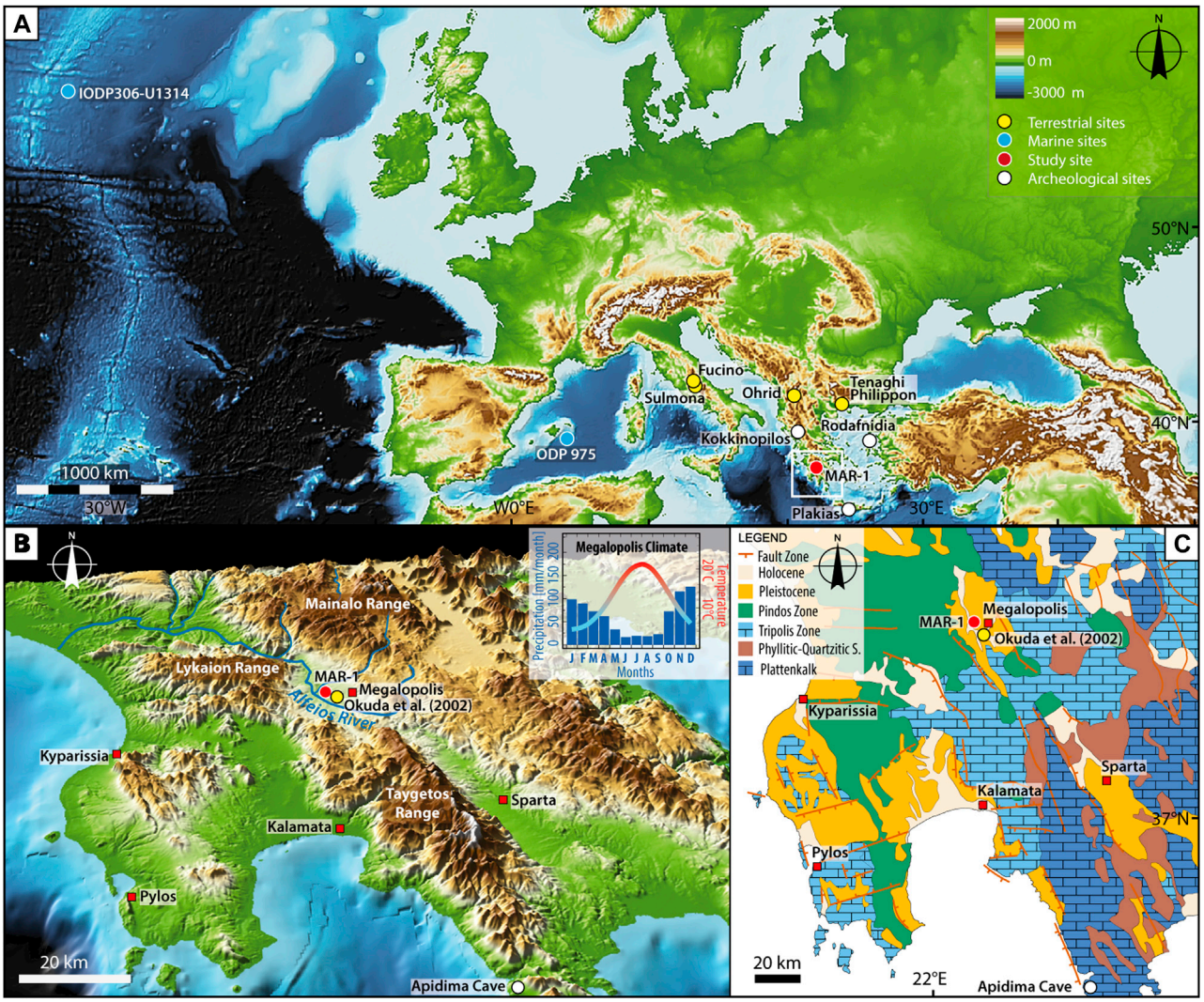

FIGURE 1 | Geographical and geological setting of MAR-1. **(A)** Overview map of Europe and the North Atlantic with sites mentioned in the text. MAR-1 is located at 37.24°N and 22.05°E. **(B)** 3D image of SW-Central Peloponnese (by GeoMapApp) showing the location of the archeological site MAR-1 (red circle) and pollen record by Okuda et al. (2002) (yellow circle) in the Megalopolis Basin. The insert shows 40-years climate average of the study region (http://iridl.ldeo.columbia.edu). **(C)** Geological map of SW-Central Peloponnese modified after Kleman et al. (2016) for the website http://www.borntraeger-cramer.de/journals/zfg.

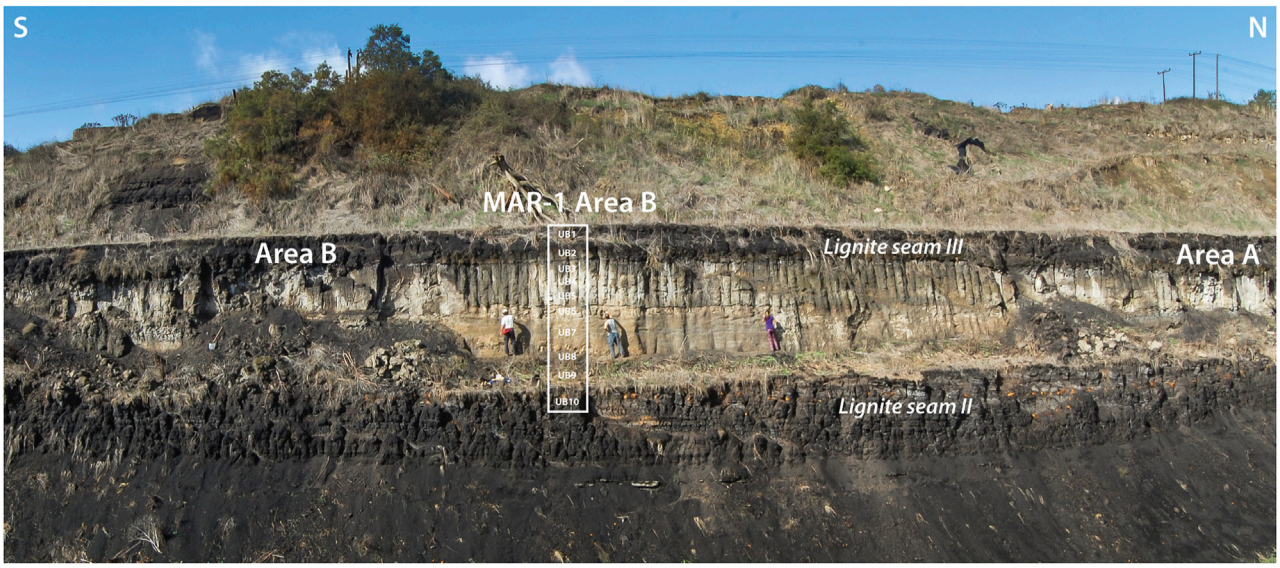

FIGURE 2 | Panoramic view of the section profile at MAR-1 with excavation areas A and B between the lignite seams LGII and LGIII. The white box marks the sampling area and indicates the distribution of the stratigraphic units UB1 to UB10.

clastic and lignite layers, rich in fossil flora and fauna, reaching back to ~780 ka (Mädler, 1971; Sickenberg, 1975; van Vugtet al., 2000; Siavalas et al., 2009; Karkanas et al., 2018; Tourloukis et al., 2018a). During a systematic survey of the Megalopolis Basin in 2013, the Lower Paleolithic archeological site of MAR-1 was discovered between the upper two lignite units (LGII and LGIII, **Figure 2**) at the northwestern margin of the basin with an age of ~480–420 ka (Tourloukis et al., 2018a; Thompson et al., 2018). MAR-1 is the first excavated archeological site in mainland Greece with a stratified assemblage of large mammals (e.g., elephants, hippos, cervids, bovids) and lithic artifacts attributed to the Lower Paleolithic (Panagopoulou et al., 2015; Panagopoulou et al., 2018; Tourloukis et al., 2018b; Konidaris et al., 2018; Thompson et al., 2018). The remains of the straight-tusked elephant *Palaeoloxodon antiquus* are especially notable, as the bones bear cut marks that have been interpreted as evidence of butchering activity by early hominins (Konidaris et al., 2018). The subsequent studies of the sedimentary structure and the spatial taphonomy of the finds indicate that they have an autochthonous origin, with the material being probably subjected to minimal post-depositional transport, most likely in the form of a hyperconcentrated flow (Tourloukis et al., 2018b; Giusti et al., 2018; Karkanas et al., 2018).

A recent magnetostratigraphy-based study correlated a number of commercial drill logs and two new outcrop sections in order to place MAR-1 in the geological sequence of the Megalopolis Basin; two age models were produced based on correlations of the Brunhes-Matuyama boundary and six chronostratigraphic surfaces to the astro-chronologically calibrated $\delta^{18}O$ benthic isotope record: according to the preferred age model, the sedimentary sequence at MAR-1 correlates to MIS12 at ~480–420 ka (Tourloukis et al., 2018a). This interval is known for its severe glacial conditions (e.g., Ermolli et al., 2010; Francke et al., 2016; Regattieri et al., 2016), making it remarkable to find indications for hominin activities in this time range. However, no high-resolution investigations of the local paleoenvironmental conditions before, during and after the deposition of human activities have been conducted so far, in order to assess if, how and when the Megalopolis Basin could have served as a refugium. Here we present a multi-proxy high-resolution study consisting of micropaleontological and geochemical analyses on a 6 m sequence directly adjacent to excavation Area B, MAR-1. The study aims at producing a continuous local reconstruction of water levels of the Marathousa paleo-lake in response to regional and global climate changes, offering additional information on the environmental backdrop of the hominin presence, and further chronological constraints for the archeological remains.

GEOGRAPHICAL SETTING

Catchment Geology

The Megalopolis Basin, situated on the central Peloponnese in southern Greece, is an intramontane half-graben basin (**Figure 1**), which formed during the Pliocene and is currently one of the largest coal mining districts in Greece (e.g., Vinken, 1965; Karkanas et al., 2018). The NNW-SSE oriented elliptically shaped basin has a maximum extension of 18 km at an altitude of 330–450 m above sea level (a.s.l.). The basin itself comprises elongated NNW-SSE-running hills and almost flat areas with slope inclinations of 0–25% and covers ~250 km^2. It is bounded by the mountain ranges of Mainalo to the east (1,981 m a.s.l.), Lykaion to the west (1,421 m a.s.l.) and Taygetos to the south (2,404 m a.s.l.).

The northeastern catchment of the Megalopolis Basin consists of the Plattenkalk series (Permian–Eocene, possibly Oligocene;

TABLE 1 | Geology of the Megalopolis Basin according to Tsiftsis (1987), [1]Dornsiepen et al. (2001), [2]Baltatzis and Katagas (1984), [3]Lekkas et al. (2002).

Stage	Group	Formation-unit	General lithology	Mineral composition (besides others)	Outcrops in the Megalopolis Basin	Other characteristics
Permian to Eocene/ Lower Oligocene[1]	Plattenkalk Series	N.A.	Crystaline, cherty limestone and phyllite, flysch	N.A.	NE	N.A.
Carboniferous to Lower Triassic[2]	Phyllitic-Quartzitic Series	N.A.	Metamorphic rocks, phyllite, mica-schist, quartzitic schist and quartzite	Carbonate, chlorite, epidote, glaucophane, graphite, mica, sphene, tourmaline, zircon	E, SE	N.A.
Upper Carboniferous to Lower Triassic[3]	Tripolis Zone	Tyros beds	Graphitic limestone, sandy micaceous limestone, (calcareous) phyllite	Brucite, carbonates, Fe-oxide/-hydroxide, feldspar, limestone, mica, quartz, sericite	NE	N.A.
Upper Triassic to Upper Eocene		Limestones and dolomites	Uniform marine dolomite, (dolomitic/bituminous) limestone, basal conglomerate, bauxite	Carbonates	E, far NE, bottom of Lousios river valley	N.A.
Upper Eocene to Upper Oligocene/ Lower Miocene		Flysch	Sandstone, shale, (marly) siltstone, (bituminous) limestone with cherts, conglomerate (sandstone, radiolarite, basic igneous rock, bauxite (local)	Carbonates, minerals contained in pebbles and conglomerates of other groups	E, far N, both sides of the Lousios river valley	Reddish-brown limonitic crust due to pre-flysch weathering, olistoliths
N.A.	Tectonic block	Tectonic block	Mélange of tripolis and pindos zone (sandstone, chert, igneous rock, conglomerate, limestone…)	N.A.	Base of Pindic nappe	N.A.
Upper Cretaceous (Cenomanian to Turonian)	Pindos Zone	The 'First Flysch'	Chert, cherty pelite/clay, fine-grained sandstone, small bodies of basic igneous rock (spilite and diabase)	Quartz, mica, feldspar, chlorite, minerals in: cherty, basic igneous rock, limestone, recrystallised fossils	NW, W	N.A.
Upper Cretaceous (Turonian to Maastrichtian)		Upper Cretaceous limestones	Limestone, pelite, chert, silt-/sand-size limeclast	Calcite, dolomite, Fe-oxide, mica	E, SE, NW, W	Stylolithes very common
Upper Cretaceous (Upper Maastrichtian) to Paleocene		Flysch	Limestone, marly limestone, chert, clastic-bioclastic limestone containing fragments of cherty rocks, basic igneous rock, grains of garnet	Calcite, carbonate, garnet	NW, W	N.A.

Dornsiepen et al., 2001) containing crystalline, cherty limestones, as well as phyllites and flysch (**Figure 1**, **Table 1**; Tsiftsis, 1987). In the SE and S of the basin, the Phyllitic-Quartzitic Series (Carboniferous–Lower Triassic; Baltatzis and Katagas, 1984; Tsiftsis, 1987) crops out. It is composed of metamorphic rocks, phyllites, schists and quartzites, containing chlorite and sphene (Tsiftsis, 1987). In the E, NE and N, the formations of the Tripolis Zone are encountered. The base of the Tripolis Zone is marked by the Tyros Beds which consist of graphitic or sandy micaceous limestones and phyllites (Upper Carboniferous–Lower Triassic; Tsiftsis, 1987; Lekkas et al., 2002). These are followed by limestones and dolomites of the Upper Triassic to Upper Eocene. The youngest parts of the Tripolis Zone are fine to medium grained sandstones, shales, limestones and conglomerates of the Tripolis Flysch (Upper Eocene–Upper Oligocene, Miocene; Tsiftsis, 1987). Outcrops of the Pindos Zone (Lower Cretaceous-Paleocene) can be found in the W and NW, as well as E and SE of the catchment (Tsiftsis, 1987). The oldest part of the Pindos Zone is the so-called "First Flysch" from the Lower Cretaceous, consisting of fine-grained sandstones, radiolarites and in some places, small bodies of igneous rocks (Tsiftsis, 1987). It transitions into Upper Cretaceous limestones and eventually into the Pindos Flysch with its cherts and limestones and in some areas into basic igneous rocks.

During the Pleistocene, lacustrine and fluvial sediments were deposited, including the lignite-bearing Marathousa Member (**Figure 2**). The Marathousa Member has a total thickness of ~150 m at the center of the basin and spans the Middle Pleistocene (Lüttig and Marinos, 1962). Its limnic and swampy sediments show complex lithological patterns, alternating between clastic sediments (clay, silt and sand) and 5–30 m thick dark brown lignite seams intercalated with thin clastic layers (Vinken, 1965).

The primary controlling factor of the development of the drainage system was probably tectonic activity, as indicated by the presence of fault zones and deformation structures, eventually

resulting in the establishment of the Alfeios River system, which today is characterized by a mixture of rectangular, parallel and dendritic patterns flowing northwards along major fault zones (Vinken, 1965; Tsiftsis, 1987). In 2002, the Alfeios River itself was rerouted into a 7 km long channel along the western side of the lignite mine (Manariotis and Yannopoulos, 2014). Its mean annual pH value is ~7.8 and during winter it reaches a maximum of 8.4 (Tsiftsis, 1987). In addition to the Alfeios River, the basin is also supplied by a karstic aquifer characterized by waters of pH 7.7–7.8 (Daskalaki, 2002; Siavalas et al., 2009).

Local Climate

The modern-day climate in Greece is characterized by hot summers and mild winters, where the winter precipitation exceeds that of summer (**Figure 1**, Kutzbach et al., 2014). The University of East Anglia Climatic Research Unit calculated monthly climatologies based on historical data (1971–2000) for the Megalopolis region and categorized it as a Mediterranean hot summer climate (Csa, according to Köppen, 1918). Monthly temperatures reach their maximum in July (mean 21.5°C) and their minimum in January (mean 4.5°C). The annual precipitation is unevenly distributed over the year and ranges from 750 to 1,000 mm/a (Okuda et al., 2002) with the majority falling in December (~125 mm) and then gradually decreasing until June (~20 mm). Additionally, storm tracks occur mostly during winter and originate either from the N-Atlantic or from the northeast, where cold Eurasian air meets the warm air above the Mediterranean (Kutzbach et al., 2014). These storm tracks vary in their intensity and frequency from year to year, depending on large-scale circulation patterns like the North Atlantic Oscillation (NAO) and the Arctic Oscillation (AO). Strong storm tracks are associated with negative phases of NAO and AO, whereas winter droughts in contrast, correlate to positive phases of NAO and AO (Givati and Rosenfeld, 2013; Kutzbach et al., 2014).

Marathousa 1 Sediments

MAR-1 extends over 92 m along the N-S axis and is divided into excavation Area A and Area B (**Figure 2**). At Area A, a dense accumulation of bones belonging to a single individual of the European straight-tusked elephant was found, as well as lithics and other faunal remains (Panagopoulou et al., 2015, 2018; Konidaris et al., 2018). The remains occur at ~349 m a.s.l. and cover ~87 m^2. Area B is dominated by a greater diversity and density of lithics together with other faunal remains. It is located 60 m south of Area A and covers ~78 m^2 at ~350 m a.s.l. Both areas contain fossils of micro- and macro-fauna and flora such as hippos, elephants and rodents, as well as seeds, fruits, and charcoal (Doukas et al., 2018; Field et al., 2018; Konidaris et al., 2018; Michailidis et al., 2018). Karkanas et al. (2018) subdivided the stratigraphy of MAR-1 into sedimentary units separated by an erosional contact into two major sequences, with the lower showing a coarsening upward and the upper a fining upward trend (**Figure 3**). At Area B, where the most complete sequence is better exposed and accessible, the lower part encompasses UB10 to UB6, with UB10 consisting of black lignitic clay that is transitioning gradually into UB9. On top of it, UB9 is mainly characterized by dark grey, massive and organic rich clayey sands, but also contains thin, wavy and ripple bedded sand laminae. The unit has been identified to be, at least partly, the result of sub-aqueous hyperconcentrated flows by Karkanas et al. (2018). The transition from UB9 to UB8 and later to UB7 is gradual. Both, UB8 and UB7, strongly resemble each other with light grey, wavy to lenticular bedded, sometimes massive fine silts and sands with deformation structures at their base. The three units UB9 to UB7 are reported to have been influenced either by waves or by storm events (Karkanas et al., 2018). The lower, coarsening upward sequence is capped by UB6 with its bluish-grey, massive muddy sands with deformation structures and mud cracks on top. The contact between the lower (UB10–UB6) and the upper sequence (UB5–UB1) is of erosional nature, with UB6 being completely eroded laterally in some parts of the site. Karkanas et al. (2018) identified this boundary to be a scour surface, i.e., it is most likely a localized erosion. Based on luminescence data from the excavation, they also conclude that the resulting hiatus does not produce a statistically significant time gap (Jacobs et al., 2018; Karkanas et al., 2018). The upper part of the sequence contains units UB5–UB1 and is dominated by the influence of mudflows and to a lesser extent by fluviatile flows (Karkanas et al., 2018). The units UB5–UB2 are very similar to each other as all contain dark grey massive and organic-rich silty and muddy sands, as well as showing an internal fining upward trend. UB5–UB3 are also characterized by an intraclast-rich base. These intraclasts are explained as partly eroded lithified sediment from the surrounding area and partly reworked material from the underlying units (Karkanas et al., 2018). An erosional contact, as well as a thin layer with mud cracks separates UB5 and UB4, indicating an exposure of the mudflat. The base of UB4 represents the fossil-rich horizon of Area B. UB4 and UB3 are both slightly eroded at their top. A scouring surface separates UB3 from UB2, the latter also containing a large amount of shell fragments. The whole sequence is capped by the black lignite and lignitic clay with a sandy component of UB1. The transition from UB2 to UB1 is gradual with local sand-rich channels.

MATERIALS AND METHODS

Sampling and Grain Sizes

A cleaned 6-m thick profile, 3 m north of Area B at MAR-1, was sampled in 5-cm intervals (**Figure 2**, **Figure 3**). The sediment profile was subdivided into ten units, UB1–UB10 (young to old), according to lithological changes as described by Karkanas et al. (2018). For the determination of grain sizes, 33 samples were cleaned following standard protocols, using 30% H_2O_2 to remove organic matter (OM) and 10% HCl to remove carbonates. The remaining solution was dispersed with ultrasonic sound and wet sieved through a 63 μm mesh. The fraction >63 μm and <63 μm were freeze dried and their weight was determined. The grain size distribution in sediments is influenced by a variety of factors, such as the depositional environment (Dearing, 1997; Digerfeldt et al., 2000; Chen et al., 2004; Liu et al., 2015; Mannella et al., 2019). Coarse grain sizes might reflect high-energy deposits like heavy precipitation-induced river

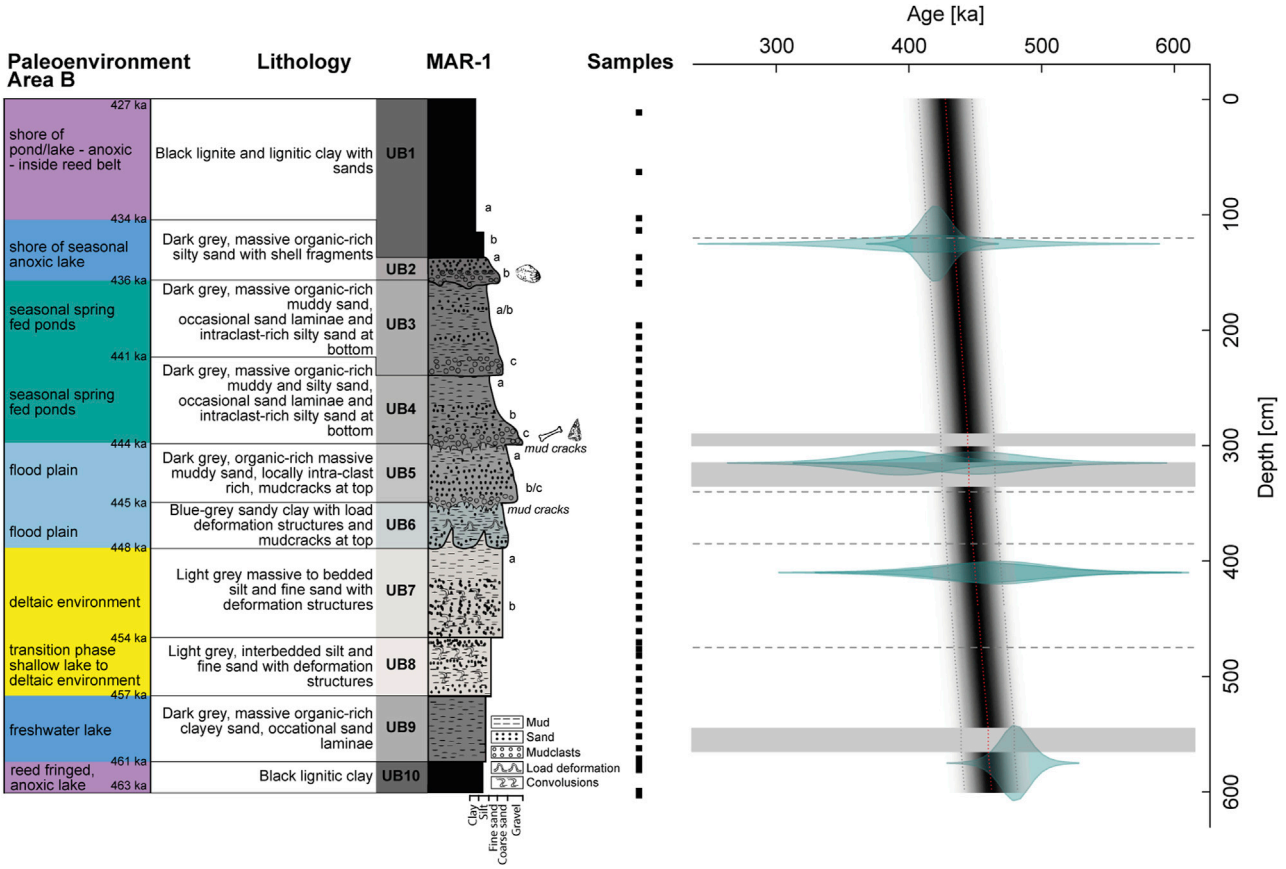

FIGURE 3 | The paleoenvironmental interpretation, sample positions and age-depth model (Bacon v2.3.9.1) (this study) in context with the lithological description from Karkanas et al. (2018) of MAR-1 Area B. Right panel: age-depth model. Grey shades: calculated ages (darker indicates more likely ages). Dotted lines: 95% confidence interval. Dashed lines: sequence boundaries. Grey bars: slump structures. Transparent green: input ages with error margins.

TABLE 2 | Overview of input ages of MAR-1 age model.

Depth (cm)	Age	Error (ka)	Reference
125	420	10	Tourloukis et al. (2018a)
125	415	46	Jacobs et al. (2018)
315	451	35	Jacobs et al. (2018)
315	394	32	Jacobs et al. (2018)
410	457	39.5	Jacobs et al. (2018)
410	468	34	Jacobs et al. (2018)
575	480	10	Tourloukis et al. (2018a)

input (Liu et al., 2015; Mannella et al., 2019), while fine grains may indicate low-energy environments (Mannella et al., 2019). This study applies a simplified approach with a division of the grain sizes in coarse (>63 μm) and fine (<63 μm) fractions. Based on those assumptions about the environmental energy, the implied distance to the shore, the transport mechanism and the water level of the potential water body are made.

Chronology

In order to better constrain the different sedimentary units of UB1–UB10, a Bayesian age model for MAR-1 was computed using the age-modelling software rBacon v2.3.9.1, written in R. Based on conclusions by Tourloukis et al. (2018a), the starting point of the sequence was set to 480±10 ka and the upper end to 420±10 ka; no additional tie points were used. Tourloukis et al. (2018a) suggested two different intervals for the deposition of MAR-1, assigning the sequence between the base of UB9 and the top of UB2 to either the glacial Marine Isotope Stage (MIS) 12 (480–420 ka) or to MIS14 (560–530 ka) based on a combination of magnetostratigraphy of the Marathousa member, chronostratigraphical correlations, and classical oxygen isotope variability by Lisiecki and Raymo (2005). The MIS12 option is the preferred model, because it also agrees with the pMET-pIRIR dating method by Jacobs et al. (2018) from the same outcrop, as well as with the small mammal biochronology by Doukas et al. (2018) (**Table 2**). (Blackwell et al., 2018) published ESR data from the upper part of the MAR-1 sequence correlated with UB2 and UB4, respectively. Their data suggested an early MIS13 age, and therefore an interglacial period for this part of the sequence. The estimated ages are not compatible with any of the other dating models proposed by Tourloukis et al. (2018a). In addition, based on findings by numerous studies such as Nickel et al. (1996) (van Vugt et al., 2001), or (Okuda et al., 2002), we also agree that the clastic intervals of the Marathousa Member probably

TABLE 3 | Input parameters for the Bacon age model and the environmental interpretation based on this study and lithological descriptions by Karkanas et al. (2018).

Unit	Boundaries (cm)	Interpretation	Sedimentation rate (mm/a)	Reference list	Acc. Shape	Acc. Mean (a/cm)	Mem. Mean	Mem. Strength	Assumed sedimentation
UB1	120–0	Swamp-like environment, reed belt	0.18	A	1.4	55	0.7	4	Continuous
UB5—UB2	340–120	Seasonal pond close to river mouth	0.17	A	8	60	0.1	20	Variable
UB6	385–340	Flood plain	0.15	B	4	65	0.7	4	Continuous
UB7	475–385	Riverine	0.14	B	8	70	0.1	20	Variable
UB10—UB8	600–475	Reed fringed, anoxic lake	0.13	B	1.6	75	0.7	4	Continuous

Bacon code

Bacon (core = "MAR1B", thick = 5, d.min = 0, d.max = 600, d.by = 5, sep = ",", dec = ".", depth.unit = "cm", age.unit = "a", ccdir = "," BCAD = FALSE, acc.shape = c (1.4,8,4,8,1.6), acc.mean = c (55,60,65,70,75), slump = c (290,300,315,335,545,565), boundary = c (120,340,385,475), mem.mean = c (0.7,0.1,0.7,0.1,0.7), mem.strength = c (4,20,4,20,4), runname = "F1_134", ssize = 2000, cc = 0)

Reference list for Acc. Mean and sedimentation rates

A	Fuccino:	Giaccio et al. (2019)	B	Dead Sea:	Kagan et al. (2018)	Lake Ohrid:	Francke et al. (2016)
	Lake Ohrid:	Panagiotopoulos et al. (2020)		Eastern Africa:	Trauth et al. (2015)	Lake Superior:	Kemp et al. (1978)
	Lake Superior:	Kemp et al. (1978)		Fuccino:	Giaccio et al. (2019)	Megalopolis:	Tourloukis et al. (2018a)
	Megalopolis:	Okuda et al. (2002); Tourloukis et al. (2018a)		Glenhead:	Blaauw and Christen (2011)	–	–

Acc. = accumulation Mem. = memory

correspond to cold (glacial) stages, while the lignite seams should represent warm (interglacial) periods. Although we cannot rule out the possibility that the ages presented by (Blackwell et al., 2018) are correct, they cannot be included in the same age model with the other ages.

During the Bayesian age modeling, rBacon divided the profile (600 cm) into 5-cm slices (*thick*). A gamma distribution based on the input parameters describes the sedimentation rates (*a/cm*; **Table 3**). Other general age-model settings of Bacon included the age (*age.unit*) and depth (*depth.unit*) units, which were set to *years* and *cm*, respectively. The calculated output ages were set in rBacon to years before AD 1950 (BP), as well as the confidence interval (*prob*) to report of 95%. Additionally, no calibration curve (*cc = 0*) was used, as the input ages were based on the potential time intervals identified by Tourloukis et al. (2018a). For the high-resolution age model, the whole profile was segmented into five different depositional environments divided by boundaries (*boundary*). For each of them, a rough framework, concerning their sedimentation behavior was estimated, based on numerous published records with similar sediments (e.g., Frogley, 1998; Okuda et al., 2002; Blaauw and Christen, 2011; Trauth et al., 2015; Francke et al., 2016; Wagner et al., 2019) that also concur with the sedimentation rates already suggested for the Megalopolis Basin (**Table 3**; Okuda et al., 2002; Tourloukis et al., 2018a; Van Vugt et al., 2000).

Based on the sedimentology the first segment (600–475 cm) was assumed to represent a reed-fringed lake that slowly changed to a deltaic, river-influenced environment. An overall low but continuous sedimentation rate was presumed (*acc.shape = 1.6, acc.mean = 75, mem.mean = 0.7, mem.strength = 4*). The next segment was considered to be dominated by a deltaic river system (475–385 cm) with a slightly higher, highly variable and unsteady sedimentation rate (*acc.shape = 8, acc.mean = 70, mem.mean = 0.1, mem.strength = 20*). For the third one (385–340 cm) the study area was assumed to have turned into a flood plain with a marginally fluctuating but continuous sedimentation (*acc.shape = 4, acc.mean = 65, mem.mean = 0.7, mem.strength = 4*). The following segment (340–120 cm) remained initially a flood plain but started to turn into a pond that was fed by a seasonal spring, with higher, highly variable and unsteady sedimentation rates (*acc.shape = 8, acc.mean = 60, mem.mean = 0.1, mem.strength = 20*). The last segment (120–0 cm) was presumed to represent a swamp-like environment within a reed belt at the edges of a lake, with continuous and high sedimentation (*acc.shape = 1.4, acc.mean = 55, mem.mean = 0.7, mem.strength = 4*). The various slumping structures (*slump*) identified by Karkanas et al. (2018) were narrowed down to three events at 565–545 cm, 335–315 cm and 300–290 cm, that were incorporated into the model (**Figure 3**, **Table 3**).

Silicate Microfossils, Ostracods and Other Microscopic Components

Silicate (SiO_2) microfossils, in particular diatoms and sponge spicules were analyzed in 47 samples following the protocol of Battarbee (1986). The morphological identification was performed at 400x and 1000x magnification using an Olympus BX51 light microscope as well as a Phenom XL Desktop Scanning Electron Microscope. Diatoms provide the potential to better constrain limnological parameters such as nutrients, pH, conductivity, clearness of the water and relative distance to the shore. Occurrences of sponge spicules are recorded in sediments of many freshwater habitats (Harrison, 1988). The skeletons of freshwater sponges are comprised of siliceous structures and are chemically identical to diatom frustules, which makes them resistant to decomposition under most conditions (Frost et al., 2001). The disintegrated skeletal network of freshwater sponges is composed of needle shaped spicules and spherical gemmules.

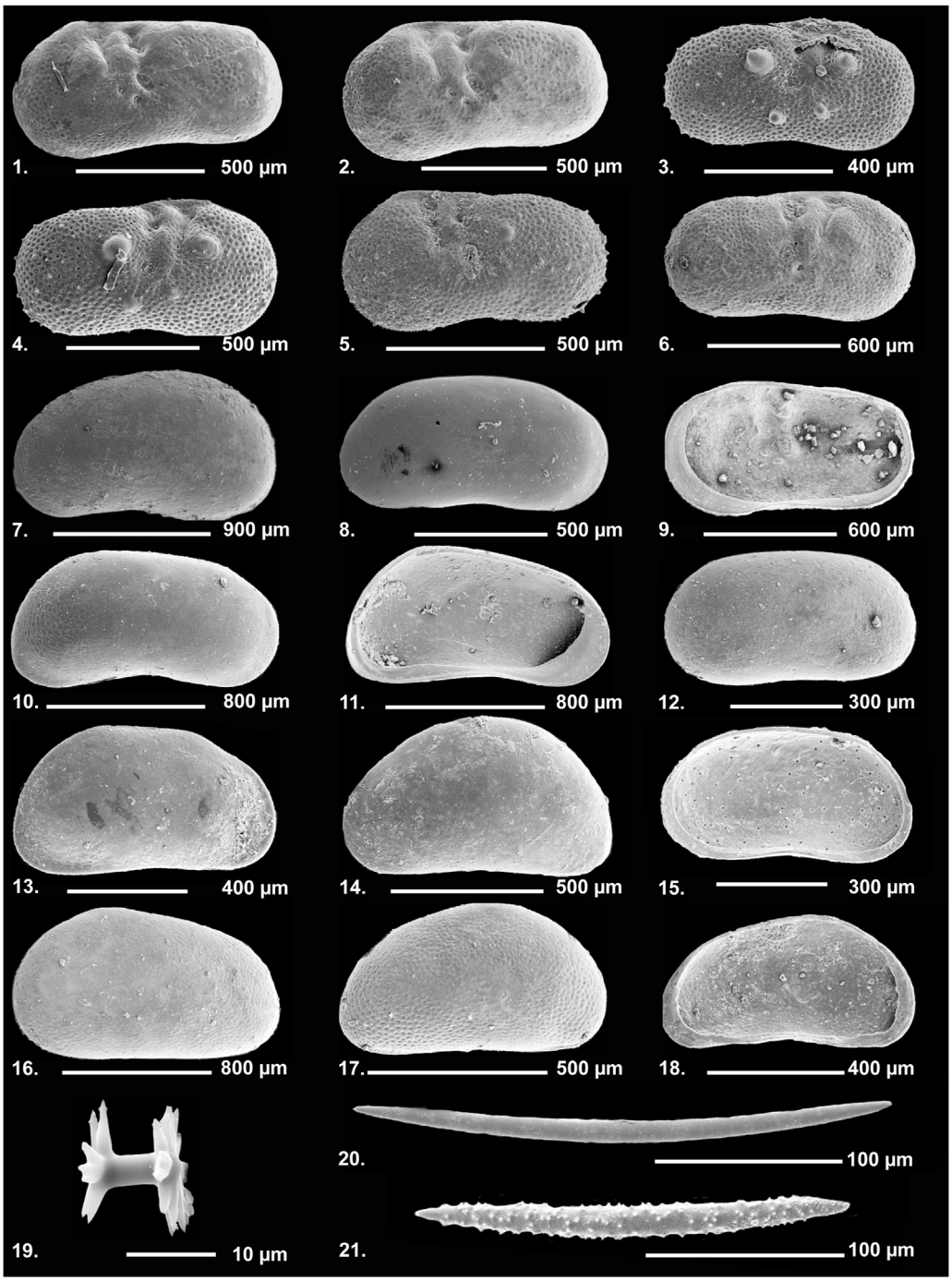

FIGURE 4 | SEM images of ostracods (1–18) and sponge spicules (19–21) from Marathousa-1 Area A and Area B. RV = right valve, LV = left valve, A = adult, im = immature, fem = female, m = male, ext = external view, int = internal view. 1) *Ilyocypris getica*, LV, a, fem, ext. 2) *I. gibba*, LV, a, fem, ext. 3) *I. gibba*, RV, im, ext. 4) *I. decipiens*, RV, im, ext; 5) *I. decipiens*, LV, im, ext; 6) *I. bradyi*, RV, a, fem, ext. 7) *Candona neglecta*, LV, a, m, ext. 8) *C. neglecta*, RV, im, ext; 9) *I. bradyi*, RV, a, fem, int. 10) *Neglecandona altoides*, RV, a, fem, ext. 11) *N. altoides*, RV, a, fem, int. 12) *Candona* sp., LV, im, ext. 13) *Pseudocandona marchica*, RV, a, m, ext. 14) *Psychrodromus* sp., LV, im, ext. 15) *Candona* sp., RV, im, int. 16) *Prionocypris zenkeri*, LV, a, fem, ext. 17) *Potamocypris zschokkei*, RV, a, ext. 18) *P. zschokkei*, LV, a, int. Sponge spicules: 19) Gemmoscleres. 20) Megascleres. 21) Microscleres.

Sponges generally require relatively clean-water conditions to sustain the filtering of their water processing system additionally to their potential algal symbionts, who require access to light (Frost et al., 2001). In this study, we used the abundance of sponge spicules and diatoms to evaluate the habitat conditions for organisms.

TABLE 4 | Ostracods and sponges.

Ostracod species	Habitat	Occurence	Reference
Neglecandona (formerly *Candona*) *angulata*	Halophilic; lives in permanent brackish waters with upper salinity limits of 13.4% that derive from small streams and springs	UB3	De Decker (1979), Fuhrmann (2012), Meisch et al. (2019)
Candona neglecta	Oligothermophyllic; inhabits low salinity water (salinity 0.5–16‰) deriving from small streams, ponds and springs; resistant taxon that can even survive desiccation	UB4	Meisch and Wouters (2004), Wagner (1957)
Ilyocypris bradyi	Oligothermophyllic; lives in flowing water of springs or where these waters runoff	UB4	Fuhrman (2012)
Ilyocypris decipiens	Freshwater or low salinity environments with a temperature range between 14 and 20°C	UB3	Meisch (2000)
Ilyocypris getica	Common in mediterranean environments; it can survive extreme conditions but has a typical temperature range of 10–15°C	UB3, UB4	Fuhrmann (2012)
Ilyocypris gibba	Freshwater to oligohaline; has an upper salinity limit of 5% and can withstand temperatures not lower than 10.5°C; can often be found in areas with swampy vegetation	UB4	Devoto (1965)
Neglecandona altoides	Lives mostly in permanent small water bodies; can also be found in temporary ponds which desiccate in summer	UB2, UB3, UB4	Fuhrmann (2012)
Potamocypris zschokkei	Found in springs	UB3, UB7	Fuhrmann (2012)
Prionocypris zenkeri	Shallow slowly flowing vegetated waters	UB4	Fuhrmann (2012)
Pseudocandona marchica	Lacustrine; can also be found in ponds	UB4	Devoto (1965)
Sponge spicule type	**Morphology**	**Occurence**	**References**
Gemmoscleres	Needle-like, dumbbell-shaped, spined or smooth, great variations in the shape of their ends; 8–300 µm, essential for the identification of freshwater sponges	UB4, UB7	Frost et al. (2001), Reiswig et al. (2010)
Megascleres	Needle-like, smooth or spined, and with a moderately high relief; 150–450 µm	UB1-UB9	Frost et al. (2001), Reiswig et al. (2010)
Microscleres	Needle-like, dumbbell-shaped; variations in presence and form of spines; do not occur for every species; 8–130 µm	UB3, UB5, UB7	Frost et al. (2001), Reiswig et al. (2010)

Ostracods and other microscopic remains larger than 125 µm were analyzed in 47 samples (12 from Area A, UA1–UA4; 35 from Area B, UB1–UB10; **Figure 3**). 500 g of dry sediment was treated with 10% H_2O_2 until reaction stopped (3–24 h). The residues were washed through a 2 mm and 125 µm sieve using distilled water and dried at 50°C. All microfossils (ostracods, gastropods and opercula, charophyte gyrogonites, thecamoebians, fish bones/teeth) were extracted under OPTIKA stereoscopes. Ostracods were further photographed using a JEOL 6300 Scanning Electron Microscope (**Figure 4**). Identification, ecology and distribution information of ostracod species were derived mainly from Danatsas (1994), Meisch (2000), Frenzel et al. (2010), Fuhrmann (2012), Mazzini et al. (2014) and several papers of the Stereo Atlas of Ostracod Shells (Athersuch et al., 1973-1996). The number of species is an indicator of the stability of the system. Taphonomic indices for the dominant species were calculated and interpreted after Schellenberg (2007) (**Table 5**) with: a) The adult to juvenile ratio (A/J) as an indirect indication for the energy of the environment. Values between 0.125 and 0.25 are typical for *in situ* death assemblages. Higher values reflect *in situ* death assemblages with taphonomic removal of juveniles. Significantly lower values could reflect transported juvenile valves or a mass death event (Belis, 1997; Schellenberg, 2007). b) The right valve/left valve ratio (RV/LV) is also considered as an indirect proxy for the energy of the depositional environment (Breman, 1980). c) The percent articulation ratio (%Art.) is an indicator of a disturbed sediment–water interface when values are lower than the common range value of most samples (Frenzel and Boomer, 2005; Hussain et al., 2007). For certain samples and species no taphonomic indices were applied, as the total number of valves per sample was too low.

X-Ray Fluorescence Analysis

Conventional X-ray fluorescence analysis (XRF) of major oxides (SiO_2, Al_2O_3, Fe_2O_3, CaO, MgO, K_2O, Na_2O, TiO_2, MnO, P_2O_5) and further trace elements (Ba, Co, Cr, Ni, Rb, Sr, V, Y, Zn, Zr, La) was applied to a total of 25 samples from all units. The sediment was first ground to powder, then mixed with 7.5 g MERCK spectromelt A12 (a mixture of 66% Li-tetraborate and 34% Li-metaborate) and melted at 1,200°C to fused beads using an Oxiflux system from CBR Analytical Service. Measurements were collected using a Bruker AXS S4 Pioneer XRF device (Rh-tube, 4 kW). Analytical errors were in the range of 10% (Relative Standard Deviation, RSD). To achieve the elemental proportions of each oxide, the weight-percentages were multiplied by a conversion factor[1] following **equation 1**, with n describing the amount of substance (mol), m_1 the amount of the individual element (wt%), m_2 the mass of the oxides from the XRF analysis and M the molar mass (g mol^{-1}).

$$n = \frac{m}{M} \leftrightarrow \frac{m_1}{M_1} = \frac{m_2}{M_2} \leftrightarrow m_1 = m_2 * \frac{M_1}{M_2} \quad (1)$$

$$\text{Example: } m(Si) = m(SiO_2) * \frac{M(Si)}{M(SiO_2)}$$

For paleoenvironmental interpretation, single element distributions and ratios are commonly used (e.g., Rothwell and Croudace, 2015; Longman et al., 2019).

Organic Carbon and Nitrogen Content

Concentrations of total carbon (TC) and total nitrogen (TN) were measured on 45 powdered samples (39–42 mg weighed into tin

[1]https://www.sciencegateway.org/tools/fwcal.htm

TABLE 5 | Ostracod taphonomy.

Area B				*Neglecandona altoides*			*Candona neglecta*			*Candona* spp. *juveniles*	
Unit	**Sample**	**Depth (cm)**	**Age (ka)**	**A/J**	**%Art**	**RV/LV**	**A/J**	**%Art**	**RV/LV**	**%Art**	**RV/LV**
UB2	Nr 1 UB2	102	433	–	–	–	–	–	–	–	–
UB2	MAR 04—CZ/TM	125	434	–	–	–	–	–	–	–	–
UB4	Nr 3 UB4	192	438	–	–	–	–	–	–	15	–
UB3	MAR 07—CZ/TM	215	440	–	–	–	–	–	–	7	0.5
UB3	MAR 08—CZ/TM	235	441	–	–	2.0	–	6	1.3	–	–
UB4	MAR 09—CZ/TM	245	442	0.8	–	2.0	–	2	1.9	–	–
UB4	MAR 10—CZ/TM	275	443	–	40	1.5	–	–	–	–	–
UB4	MAR 11—CZ/TM	295	445	4.0	67	–	5.0	67	1.0	36	1.3
UB7	MAR 18—CZ/TM	450	453	–	–	–	–	–	–	–	–
UB7	MAR 19—CZ/TM	475	454	–	–	–	–	–	–	–	–

Area A				*Neglecandona altoides*			*Candona neglecta*			*Candona* spp. *juveniles*	
Unit	**Sample**	**Elevation (m a.s.l.)**	**Age (ka)**	**A/J**	**%Art**	**RV/LV**	**A/J**	**%Art**	**RV/LV**	**%Art**	**RV/LV**
UA2	Sample 5	351.1	–	–	–	–	–	–	–	–	0.9
UA2	Sample 7	350.53	–	–	–	–	–	–	–	–	0.9
UA3a	Sample 9	349.94	–	–	–	–	–	–	–	–	–
UA3b	Sample 10	349.74	–	–	–	–	–	–	–	14	–
UA3c	Sample 11	349.71	–	–	–	–	–	–	–	–	1.0

A/J = Adult/Juvenile RV/LV = Right valve/Left valve

capsules) after combustion at 1,150°C using the Vario ELIII elemental analyzer. Approximately 39–42 g of tungsten (VI)-oxide was added to each tin capsule to guarantee stable high temperatures. Blank capsules with sulfanilic acid were used as a standard and measured three times prior to the first, after the 33rd and the final measurement, to guarantee accurate results. The percentage amount of carbon and nitrogen was calculated from its absolute gravimetric content compared to the input sample weight. If the RSD exceeded 10%, a new measurement was performed. The detection limit for TC was 0.10 wt% and for TN 0.05 wt%. The concentrations of the analysis represent the mean values of double measurements. $CaCO_3$ was determined gas-volumetrically with an Eijkelkamp Calcimeter using 0.5–2.5 g of powered sample material. $CaCO_3$ weight percentages were calculated following **Eq. 2** according to DIN 18129 with a being the volume of the produced CO_2 in cm^3, p the air-pressure in Pascal, t the room temperature in °C and E the weight of the sample material in g.

$$\frac{a \times p \times 1.204 \times 10^{-3}}{(273 + t) \times E} = wt\%CaCO_3 \quad (2)$$

The mass m (wt%) of Total Inorganic Carbon (TIC) was computed by dividing the atomic mass ratio of carbon ($M(C) = 12.00 \frac{g}{mol}$) by the atomic mass of $CaCO_3$ ($M(CaCO_3) = 100.09 \frac{g}{mol}$) and multiplying it with wt% $CaCO_3$ (**Eq. 3**).

$$m(TIC) = m(CaCO_3) * \frac{M(C)}{M(CaCO_3)} \quad (3)$$

TIC describes the amount of carbon dioxide (CO_2), carbonic acids (H_2CO_3), bicarbonates (HCO_3^-) and carbonates (CO_3^{2-}) in a sample (Rantakari and Kortelainen, 2008). The influence of H_2CO_3 is assumed to be negligible when alkaline conditions prevail. The remaining components derive from weathering of carbonates, or the production of calcifying organisms (Rantakari and Kortelainen, 2008). A good indicator of biogenic carbonates is usually a positive correlation of TIC with Ca and Sr. Total organic carbon (TOC), in contrast, describes the amount of OM, which escaped the remineralization processes during deposition (Meyers and Teranes, 2001). TOC was calculated by subtracting TIC from TC (**Eq. 4**).

$$TOC = TC - TIC \quad (4)$$

The ratio of TOC/TN (C/N) is a tool to identify the origin of OM and thus to distinguish long-term changes in the lake environment (e.g., Meyers and Benson, 1987). To yield the C/N atomic ratios that reflect biochemical stoichiometry, C/N is multiplied by 1.167 (Meyers and Teranes, 2001). Lower values of 4–10 are typical for OM based on phytoplankton, as those tend to bind high concentrations of nitrogen, whereas terrestrial, vascular plants produce values of 20 and higher. In general, most lakes have values of 10–20, indicating a mix of both vascular plants and algae (e.g., Meyers and Teranes, 2001; Cohen, 2003). The interpretation, however, must be exercised with caution, as the ratio can be influenced by multiple factors such as selective degradation or increased temperatures (Meyers and Benson, 1987; Meyers and Teranes, 2001; Cohen, 2003).

Correlation, Statistical Significance and Principal Component Analysis

In a statistical approach, the p-value for statistical significance and the Spearman correlation coefficient r_s were calculated. The p-value is used in the context of null hypothesis testing to

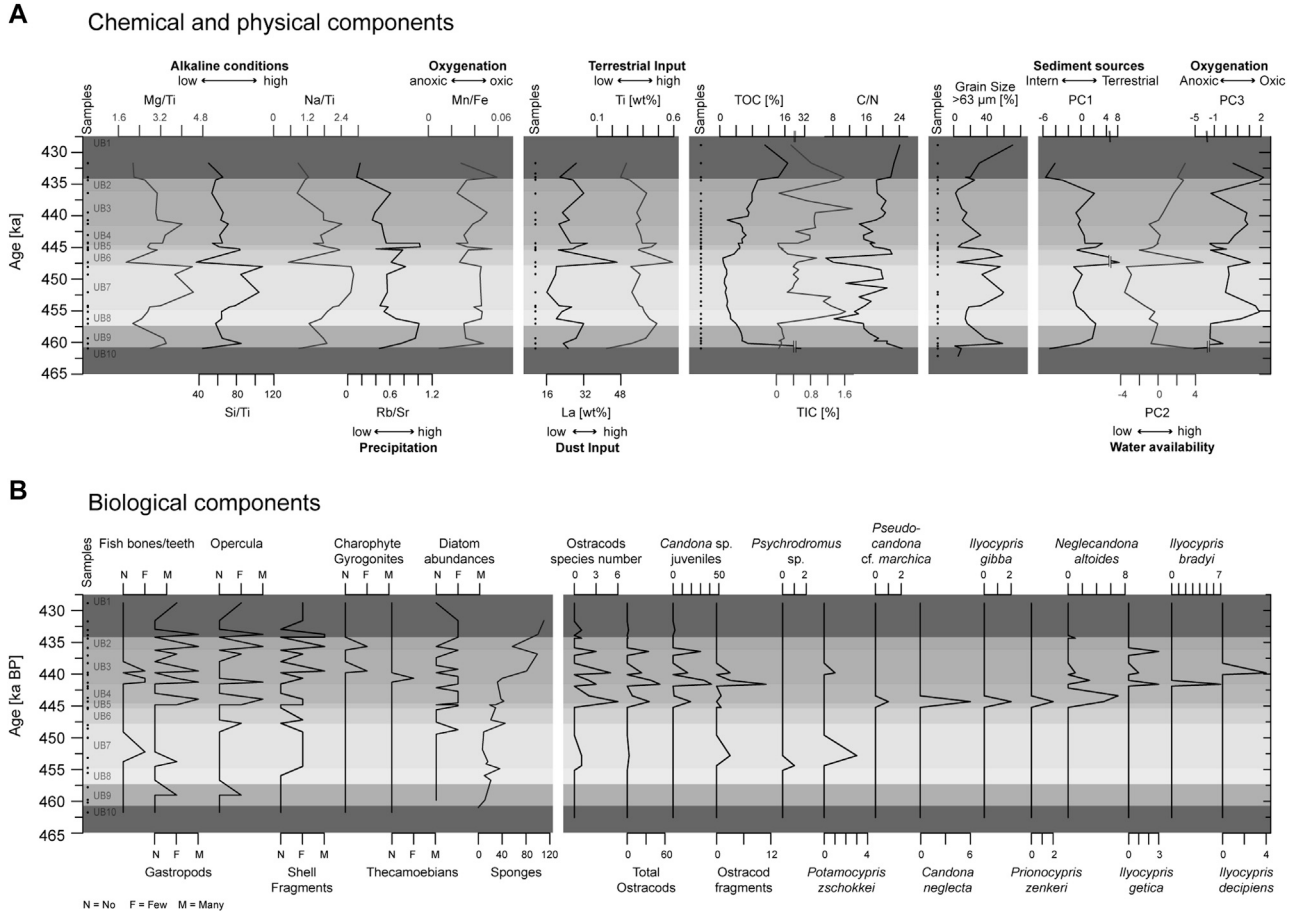

FIGURE 5 | Multiproxy data from MAR-1 Area B sediments against time. The data are divided into the categories **(A)** chemical and physical components, including the results of the PCA analysis, and **(B)** biological components.

quantify statistical significance (Bhattacharya and Habtzghi, 2002). Values of $p<0.05$ show statistical significance, but this does not always guarantee that the result is scientifically significant as well. Spearman's correlation coefficient represents the statistical dependence of two variables based on their rank (Hammer et al., 2001; Trauth, 2014). It can vary between 1 and −1, with 1 being regarded as a complete correlation and −1 as anti-correlation. Both values were determined using the software PASTv4.03 (Hammer et al., 2001). The p-value was applied to assess whether two variables are correlated at all and r_s was used to determine the degree of that correlation (Hammer et al., 2001). A principal component analysis (PCA) was used to identify patterns of similar behavior in our data sets (Abdi and Williams, 2010; Jolliffe and Cadima, 2016). The viable PCs were narrowed down by selecting only those that together described at least 80% of the variance. To ensure an ideal comparison of the various different applied techniques, only the measurements of the same depths were used. Hence, the XRF measurements were reduced from 25 to 24, TOC and TIC from 45 to 24 and grain size measurements from 33 to 24.

RESULTS

Age Model

The computed age model puts the MAR-1 sequence between 463±20 ka and 427±20 ka and thereby into the glacial MIS12 (**Figure 3**). It yielded the approximate ages for the respective units of >463–461 ka (UB10), 461–457 ka (UB9), 457–454 ka (UB8), 454–448 ka (UB7), 448–445 ka (UB6), 445–444 ka (UB5), 444–441 ka (UB4), 441–436 ka (UB3), 436–434 ka (UB2) and <434–427 ka (UB1). The model places the archeological site at ~444±20 ka. The calculated sedimentation rates vary between 0.18 mm/a (~55 a/cm) and 0.13 mm/a (~77 a/cm) (**Table 3**), which concurs with the those suggested by Van Vugt et al. (2000), Okuda et al. (2002) and Tourloukis et al. (2018a), who determined sedimentation rates between 0.1 mm/a and 0.26 mm/a.

Grain Sizes

Grain sizes fluctuate rapidly between coarse (>63 µm) and fine (<63 µm) values, with only minor steady trends from UB10–UB8 and between UB4–UB1 (**Figure 5**). The coarse-grained fraction of

the individual samples dominated samples with 56–58 wt% in UB6, UB7 and UB9, and 70 wt% in UB1. Lowest values of the coarse grained-fraction were recorded in UB10 and UB3 (2–5 wt %) as well as UB6 (4 wt%), and UB5 (6 wt%).

Silicate Microfossils, Ostracods and Other Macroscopic Components

Diatoms are very rare. Even for abundant taxa, preservation is poor in most cases, preventing them from being used for limnological interpretations of the paleo-lake Marathousa. Where identification was possible, mostly benthic or epiphytic genera, such as *Cocconeis* sp., *Cymbella* sp., *Epithemia* sp., *Fragilaria* spp., *Gomphonema* sp. and *Stauroneis* sp. were identified, indicating shallow water. A few planktonic species, such as *Cyclotella* sp., could also be identified in the upper part of the sequence. In contrast, sponge spicules were the most common silicate microfossils, occurring in nearly all units, except UB10 (**Figure 4**, **Figure 5**, **Table 4**). They were most abundant between UB4–UB1. For the further interpretation, the general occurrence of sponge spicules in the samples were used to support XRF interpretations.

The total number of ostracods in this study is in general very low, and interpretation of the assemblages should be taken with caution. Out of the 47 samples that were analyzed from Area A and B, 21 were totally barren of ostracods (UA1, UA4, UB1, UB5, UB6, UB8–UB10; **Figure 5**). The quantity of ostracod specimens per sample is highly variable, ranging between 0 and 52, with species numbers of 0–6 per sample. In total, 13 ostracods species could be identified (**Figure 4**, **Table 4**), with higher numbers occurring in samples MAR03 (115 cm, UB1), MAR05 (150 cm, UB2), MAR07 (215 cm, UB3), MAR09 (245 cm, UB4) and MAR11 (295 cm, UB4) in Area B, and in the sample of UA3b in Area A. Candonidae and Ilyocyprididae dominate the assemblage (**Figure 5**). More specifically, juvenile stages of *Candona* sp. were found in 12 samples with relatively high frequencies, reaching 51 in UA3 of Area A. Adult specimens of mainly *Neglecandona altoides* and *Candona neglecta* were only found in six samples from Area B. A representative of *Pseudocandona marchica* has been retrieved from sample MAR11 (295 cm, UB4) of Area B. As far as the number of species is concerned, *Ilyocypris* spp. exhibit the highest diversity, with four different species being identified (*I. bradyi*, *I. decipiens*, *I. getica* and *I. gibba*). They were found, however, only in low frequencies, not exceeding seven valves per sample (maximum abundance in sample MAR09, 245 cm, UB4). Several other freshwater species (*N. angulata, Darwinula* sp., *Potamocypris zschokkei*, *Prionocypris zenkeri*, *Psychrodromus* sp.) were found scattered in different samples and with very low frequencies (one to three valves per sample) (Martens and Savatenalinton, 2011; Ruiz et al., 2013; Meisch et al., 2019). Lüttig (1968), who conducted a study on the ostracods of the Megalopolis Basin, does not report several species that have been identified here (*P. zschokkei, P. zenkeri, P. marchica, I. getica, I. decipiens* and *I.bradyi*), even though an assemblage rich in Candonidae and Ilyocyprididae is mentioned.

Taphonomic indices were calculated for the Candonidae representatives and for samples with adequate number of valves (**Table 5**). As far as the juvenile *Candona* spp. of sample MAR07 (215 cm, UB3) are concerned, the low value of %Art. ratio (6.67%) and the RV/LV ratio (0.5) reveal a disturbed sediment-water interface and transported valves. Both *N. altoides* and *C. neglecta* from sample MAR11 (295 cm, UB4) have been deposited *in situ* since A/J ratios are high (4.0 and 5.0 respectively). Deposition took place under a calm sediment water interface since both %Art. ratios are high (67.0 and 66.7% respectively). However, low energy water must have transported some juvenile valves to the depositional environment since the %Art. ratio for juvenile *Candona* spp. is relatively low (35.7%). On the other hand, the RV/LV ratio for *Candona* spp. deriving from Area A (samples from UA2, UA3b and UA3c) shows no disturbed values (~1.0); however, like the UB4 juveniles, these valves are all considered transported, since no adult specimens were found. The low value of the %Art ratio (13.6%) in the sample from UA3b reveals a disturbed sediment-water interface.

Other macroscopic components were encountered in every unit, with gastropods being the most common. Gastropods and/or opercula were found in 12 samples with only a few found in UB9 and at the beginning of UB7 (**Figure 5**). Their share increases and strongly fluctuates between UB5 to UB1. The content of shell fragments behaves in a similar way with a slight increase at the end of UB7. Fish bones were few in number and only present in UB7, UB4 and UB3. Charophyte gyrogonites were noted in two samples, while fish teeth/bones and thecamoebians were observed in four and one samples, respectively.

X-Ray Fluorescence

TiO_2 and **Rb** in MAR-1 sediments are comparatively low with average values of 0.63 wt% and 77.33 ppm. Enhanced values are recorded in UB9, UB8 and UB6 and minima in UB1 and UB10 (**Figure 5**). **La** shows very low average values (25.75 ppm) and trends correlates in its maxima with TiO_2 and Rb but has a minimum in UB7. **Sr** content ranges around 156.32 ppm and starts with very low values in UB10 and fluctuates strongly around a continuously increasing trend towards UB1. **Fe_2O_3** exhibits continuously low values with an average of 4.41 wt%, one pronounced peak in UB6 and its minimum in UB1. **MnO**, with an average of 0.15 wt%, follows a strongly fluctuating trend with a maximum in UB6 and minima in UB10 and UB1. **MgO**, **Na_2O** and **SiO_2** exhibit a very similar behavior with averages of 1.88 wt%, 0.89 wt% and 54.53 wt%, respectively. Maximum values are reached in UB9, UB7 and UB5, while minima are recorded at UB10, UB6 and UB1. The ratios **Mg/Ti, Na/Ti** and **Si/Ti** show a similar trends with constantly rising values in UB8 to UB7, which abruptly change in UB6 and decrease under strong fluctuations towards the top of the sequence. **Rb/Sr** experiences an initial steep rise between UB10 to UB8 and then decreases under fluctuations towards UB1. **Mn/Fe** is strongly fluctuating with maxima at UB9, UB5 and UB1 and minima at UB10, UB4 and UB1.

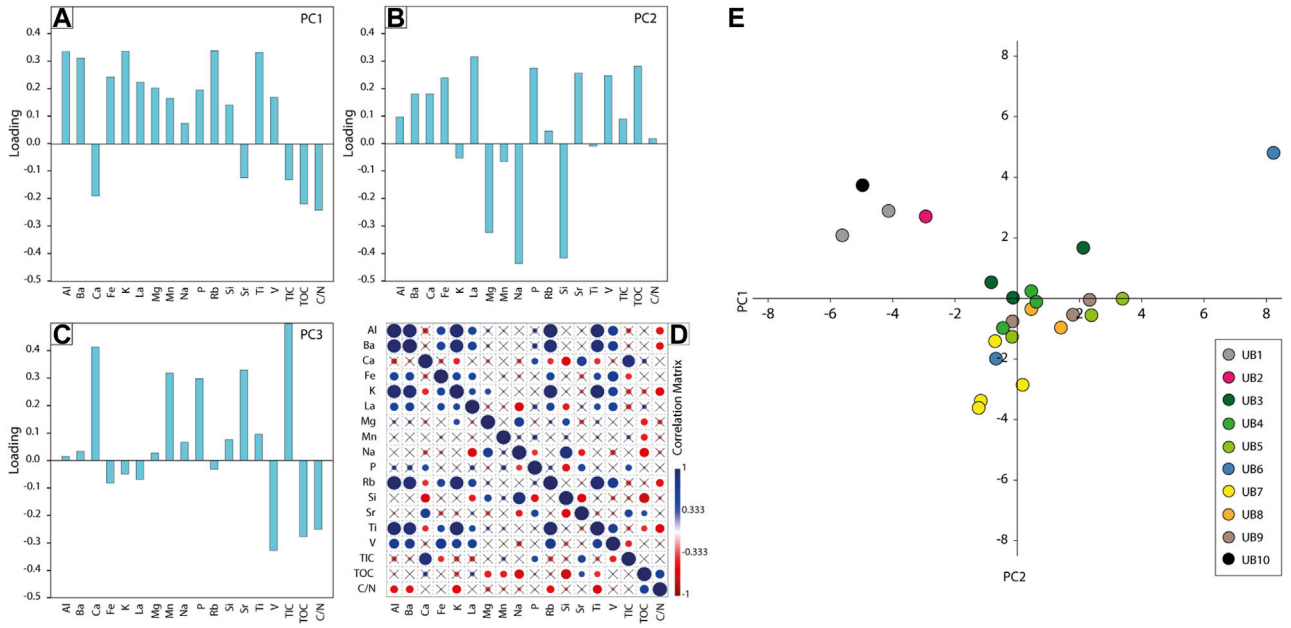

FIGURE 6 | Results of the statistical analysis. **(A–C)** Loadings of chemical components representing their influence on the computed principal components (PC1–PC3). **(D)** Correlation matrix showing the relation of the chemical components to each other. Blue indicates a positive correlation, while red shows an anticorrelation. The size of the circles is determined by the intensity of correlation. **(E)** Plot illustrating the impact of PC1 and PC2 on the lithological units.

Total Inorganic Carbon, Total organic carbon and TOC/TN Ratios

TIC is highly variable with values ranging from 0.02 wt% (UB9) to 1.77 wt% (UB3). Major peaks are encountered at the beginning of UB1 (1.58 wt%), in the middle of UB3 (1.78 wt%) and at the end of UB8 (1.62 wt%). The lowest values can be found in UB3 (0.06 wt%), UB5 (0.03 wt%) and UB9 (0.02 wt%). The calculated TOC values decline from UB10 to UB6 and subsequently increase from UB5 to UB1. TOC achieves a minimum of 0.74 wt% (UB6) and a maximum of 31.07 wt% (UB10). The C/N values in the MAR-1 sediments are highly variable, fluctuating from 6.26 up to 24.69. The ratio decreases sharply from the middle of UB6 until the boundary to UB7. In the lignite layers, the ratios are usually very high (UB1–24.09 and UB10–24.69).

Statistics Results

PCA analysis was carried out to identify the major influences on the sedimentation processes. The first three principal components (PC1-PC3) make up 85.8% of the total variance. The first eigenvalue accounts for 45.2%, the second for 25.0% and the third for 15.6%. Any other remaining component reflects less than 6.5% of the total variance. Therefore, only PC1 to PC3 were used for interpretation (**Figure 6**).

DISCUSSION

Proxy Evaluation

X-Ray Fluorescence Proxies Interpretation

Rubidium (Rb) is a conservative element mainly associated with clay minerals where it often substitutes for K (Jin et al., 2006; Kylander et al., 2011; Heymann et al., 2013). In a humid climate, the content of Rb tends to be elevated due to a high precipitation and a subsequent increase of erosion and terrestrial input (Fernández et al., 2013; Heymann et al., 2013).

Strontium (Sr) rarely forms independent minerals, but if it does, they are usually associated with sedimentary rocks (Hibbins, 2000). One source of Sr may be of biogenic production such as calcifying organisms, however due to the low amount of remains found in the MAR sediments, the share of biogenic Sr is considered negligible (Cohen, 2003; Férnandez et al., 2013). Another source could be erosion/weathering of the catchment which is largely comprised of carbonaceous rocks. Karkanas et al. (2018) determined that the sediments of MAR-1 have a very high carbonate content and microscopic analyses revealed the catchment as origin. Therefore, it is assumed that the Sr originates from the catchment (**Table 6**).

Rb/Sr ratio is usually regarded as a weathering proxy, indicating the relative humidity of the climate (Unkel et al., 2011; Fernández et al., 2013; Heymann et al., 2013; Emmanouilidis et al., 2018). A humid climate promotes erosion and the influx of Rb and also increases the chemical weathering of carbonaceous rocks, leaching Sr from the sediments (Jacobson et al., 2002; Unkel et al., 2011; Heymann et al., 2013). In contrast, a dry climate favors the deposition of Sr in sediments, due to increased erosion instead of weathering. As a result, high Rb/Sr values tend to indicate a more humid climate and low ones a drier climate. However, other processes (e.g., sedimentary sorting) can influence the proxy. Finer sediments with a higher mica-rich clay fraction often have higher Rb/Sr values, as Rb is often associated with clay minerals. Therefore,

TABLE 6 | Summary of geochemical proxies and their origin applied for the interpretation of MAR-1 sediments.

Proxy	Origin	Reference
Al	Terrestrial	Rothwell and Croudace (2015)
Ba	Biogenic	Bishop (1988), Calvert and Pedersen (2007)
Ca	Biogenic	Jouve et al. (2013), Mannella et al. (2019)
Fe	Redox	Cohen (2003), Naeher et al. (2013), Burn and Palmer (2014), Rothwell and Croudace (2015)
K	Terrestrial	Rothwell and Croudace (2015)
La	Dust	Muhs et al. (2007), Muhs et al. (2010)
Mg, Na, Si	Alkalinity, chemical weathering	West et al. (2005), Rothwell and Croudace (2015)
Mn	Redox	Davison (1993), Cohen (2003), Naeher et al. (2013), Rothwell and Croudace (2015)
Rb	Terrestrial	Jin et al. (2006), Heymann et al. (2013), Kylander et al. (2011)
Sr	Biogenic	Cohen (2003), Férnandez et al. (2013)
Ti	Terrestrial	Fitzpatrick and Chittleborough (2002), Rothwell and Croudace (2015), Regattieri et al. (2017), Mannella et al. (2019)
V	Terrestrial	Shaheen et al. (2019)
Al/Ca	Fluvial	Nizou et al. (2011)
Al/Si	Chemical weathering	Hoang Van et al. (2010)
Ba/Al	Detrital	McManus et al. (1998)
Ba/Ca	Runoff	Grove et al. (2010)
Ba/Ti	Paleo-productivity	Thomson et al. (2006)
Mg/Ti, Si/Ti	Alkalinity, chemical weathering	This study
Mn/Fe	Lake redox conditions (oxic vs. anoxic)	Koinig et al. (2003), Haberzettl et al. (2007), Naeher et al. (2013), Burn and Palmer (2014)
Na/K, Na/Ti	Alkalinity, chemical weathering	Nesbitt and Wilson (1992), Chen et al. (2001), Roy et al. (2008)
Rb/Sr	Precipitation	Unkel et al. (2011), Fernández et al. (2013), Heymann et al. (2013), Emmanouilidis et al. (2018)
C/N	Vegetation	Meyers and Teranes (2001)
TOC	Organic carbon	Meyers and Teranes (2001)
TIC	Inorganic carbon	Meyers and Teranes (2001)
PC1	Sediment sources (intern vs. terrestrial)	This study
PC2	Water availability (alkaline conditions)	This study
PC3	Oxygenation (anoxic vs. oxic)	This study

lower values are expected in coarser, feldspar-rich sediments (Hemming, 2007; Cole et al., 2009). As the composition of the sediments at MAR-1 alternates rapidly between fine and coarse sediments (ranging from 1.5 to 70% coarse fraction), the ratio of Rb/Sr has to be considered with caution and is only considered a rough proxy of precipitation. Pollen analysis can help establishing the closer relation between Rb/Sr and precipitation.

Manganese (Mn) is a highly redox sensitive element which has its origin in the surrounding catchment (Rothwell and Croudace, 2015). Under oxidizing conditions, it is encountered as insoluble Mn^{4+} and under reducing ones as soluble Mn^{2+} (Davison, 1993; Cohen, 2003; Naeher et al., 2013).

Iron (Fe) is one of the earth's most common elements and usually correlated with terrigenous markers like Ti (Rothwell and Croudace, 2015). Most commonly, it enters a lake as iron oxide or hydroxide and settles through the water column until it encounters either anoxic waters or OM, which act as a reducing agent (Cohen, 2003). (Kelepertsis and Kontis. 1997) confirm an external source for iron in the Megalopolis Basin. Under oxidizing conditions, ferric iron (Fe^{3+}) is the insoluble and stable state of iron, which is deposited (Cohen, 2003; Burn and Palmer, 2014). In anoxic waters, Fe^{3+} is reduced to the highly soluble Fe^{2+} (Cohen, 2003; Naeher et al., 2013; Burn and Palmer, 2014). However, Fe^{2+} can also be bound in pyrite (FeS_2), if enough sulfur, produced by the reduction of SO_4^{2-}, is available (Cohen, 2003).

The **ratio Mn/Fe** can be used to reconstruct the redox milieu (Koinig et al., 2003; Naeher et al., 2013; Burn and Palmer, 2014). In anoxic waters, the reduced form of Mn (Mn^{2+}) is more stable in the water column than Fe^{2+}, i.e., Fe^{2+} is more easily bound and deposited as a $FeCO_3$ or more commonly as FeS_2 (Koinig et al., 2003; Burn and Palmer, 2014). Hence, Mn/Fe ratios of anoxic sediments remain low (Burn and Palmer, 2014). In an oxic water column, Mn/Fe is high, as both Mn and Fe are precipitated (Burn and Palmer, 2014).

Titanium (Ti) is a conservative and immobile element, which typically occurs in weathering-resistant minerals (e.g., rutile, ilmenite), but can also be constituent of clay minerals (Chawchai et al., 2016; Regattieri et al., 2017). As it is not affected by diagenetic overprinting or biological processes it is often applied as an indicator for terrestrial input due to erosion and external processes (Fitzpatrick and Chittleborough, 2002; Rothwell and Croudace, 2015; Mannella et al., 2019).

Magnesium (Mg) is a major bedrock constituent, usually as carbonates, and is considered to be of detrital origin (Tsiftsis, 1987).

The primary source of **Sodium (Na)** are usually igneous and metamorphic rocks but it can also stem from clay minerals and other sedimentary rocks in the catchment (Tsiftsis, 1987). Na can be used to identify the degree of chemical weathering.

The origin of **Silicon (Si)** in sediments can be either of detrital origin such as from igneous and metamorphic rocks, volcanic ashes, or from phytoliths (part of plants; Field et al., 2018) or from aquatic organisms such as diatoms or sponges (Tsiftsis, 1987; Cuven et al., 2010).

The ratios **Na/Ti** can be regarded as a proxy for the chemical weathering of igneous rocks (Nesbitt and Wilson, 1992; Chen et al., 2001; Roy et al., 2008). A similar source is assumed for the ratios **Si/Ti** and **Mg/Ti**, as their behavior,

constantly rising values in the silts and fine sands of UB8 to UB7, which abruptly changes in UB6 and decreases under strong fluctuations towards the top of the sequence (**Figure 5**), resembles the one of Na/Ti. According to Flower (1993), the content of dissolved Na and Mg in the water column influences the preservation of siliceous organisms like diatoms and sponges. Diatom preservation is deteriorating from calcium through magnesium to sodium carbonate dominated systems due to higher dissociation constants (Katrantsiotis et al., 2016). Therefore, these ratios are interpreted to represent lake-internal dissolution processes due to changes in alkalinity.

Lanthanum (La) is a rare earth element, which has been found in high concentrations in Saharan dust (Muhs et al., 2007; Muhs et al., 2010). Evidence of the influence of Saharan dust has been found throughout the Mediterranean region (Dayan et al., 1991; Muhs et al., 2010; Remoundaki et al., 2011; Nava et al., 2012; Varga et al., 2014). Modelling studies suggested that the dust transport during the last glacial was generally higher than during interglacials and thus could yield higher La values (Mahowald et al., 2006; Williams et al., 2016). This could also be the case during older glacials, and therefore La is considered an important element in this study (**Figure 5**).

Reconstruction of Environmental Processes Using Principal Component Analysis

The parameters influencing PC1 positively (Al, Ba, Fe, K, La, Mg, Mn, P, Rb, Si, Ti and V) are mostly of terrestrial nature and must have been transported into the lake via various processes (**Figure 6**). The correlation of Al, Ba, K, Rb, V and Ti hints towards the basement exposed in the NE and NW and/or the soils as the main sediment source, whereas Mg most likely has its origin in the carbonates of the Pindos and Tripolis zone (**Figure 2**; e.g., Tsiftsis, 1987; Fitzpatrick and Chittleborough, 2002; Rothwell and Croudace, 2015; Mannella et al., 2019). Typically, flysh often contains Al-rich silicate minerals such as illites or feldspars, while altered volcanics usually contain chlorite, feldspars, hematite and are perhaps enriched in Ti and V. La possibly originates in the Sahara dust (e.g., Muhs et al., 2010; Varga et al., 2014), which was transported via air to the Megalopolis Basin. Given the strong correlation of Na and Si in the MAR-1 sediments and the positive loading of Si in PC1, a detrital rather than a biogenic source of Si is assumed. PC1 is negatively controlled by proxies which seem to reflect an origin mainly from lake-internal processes (Ca, Sr, TOC, TIC, and C/N). Since Ca, Sr and TIC are anticorrelated to the other elements, they might be associated with biogenic carbonate production within the lake or to karstic erosion of the limestones in the western basin, as Karkanas et al. (2018) suggested. However, the high loadings of TOC and C/N, which are both controlled by lake organisms, indicate that Ca, Sr and TIC are probably influenced by the same source. We thus conclude **PC1** to represent information on **external (positive scores) vs. internal sediment sources (negative scores)**.

The parameters that influence **PC2** reflect alkalinity changes of the paleo-lake water, which are known to be often related to climate-driven lake-level changes as suggested in several paleo-lake archives (e.g., Cohen, 2003; Foerster et al., 2018; **Figure 2**, **Figure 6**). The anticorrelation of the Na/Ti, Mg/Ti, and Si/Ti ratio with PC2 supports our interpretation. Alkaline waters with pH>9 are known from today's dry and carbonate-rich environment of the Peloponnese (Chatziapostolou et al., 2013; Katrantsiotis et al., 2016; Weiberg et al., 2016). Highly alkaline waters are here related to the weathering of the surrounding rocks, consisting of Na-rich albite and Mg-rich dolomite, among others (Tsiftsis, 1987). During chemical weathering, Na- and Mg-cations, among others, are released and washed into the lake water, inducing alkaline conditions (Flower, 1993). This chemical reaction is also reflected in the opposing PC loadings. Whereas negative loadings, with Mg, Na, Si dominating, reflect drier climate and alkaline conditions, more humid episodes in contrast provide a freshening of the paleo-lake system. Furthermore, the influx of a variety of elements (positive loadings with Al, Ba, Ca, Fe, P, Sr) enhance lake productivity as reflected by TIC and TOC. Based on the various influencing factors, we consider PC2 to reflect changes in the general **availability of water** in the catchment with positive scores representing high, and negative scores low water availabilities.

The positive loadings of **PC3** are dominated by Ca, Mn, P, Sr, and TIC. All parameters, except for Mn, can be found in endogenic carbonates, shells ($CaCO_3$) and fish, or other bones ($Ca_5(PO_4)_3(OH)$). Mn is related to the oxidation status of the water column, with high Mn (compared to Fe) indicating a well-oxygenated water column (e.g., Burn and Palmer, 2014). The negative loadings of PC3 are dominated by TOC, C/N and V. TOC values are high in the lignite layers, indicating anoxic sediment conditions, whereas C/N indicate input of land vegetation to the sediments during these stages. Based on the influences mentioned above, we conclude that PC3 reflects **oxic** (more positive scores) and **anoxic** (strong negative scores) conditions of **paleo-lake** Marathousa. This interpretation is also supported by the ratio of Mn/Fe, which is often used to interpret the oxidation of the water column (e.g., Koinig et al., 2003; Burn and Palmer, 2014).

Silicate Microfossil Dissolution

Only a small number of diatoms was found with most of them either heavily weathered or fragmented, from UB1 down to UB6 (**Figure 5**). In the lowest parts of the sequence, they nearly disappear completely. Field et al. (2018), who investigated Area A and parts of Area B, obtained similar results but observed also large differences between the two excavation sectors with respect to preservation. The authors concluded that the scarcity and low diversity of diatoms could be the result of lake water disturbance which affected the bottom sediments, e.g., mudflows. However, another possibility for low preservation could be alkaline conditions in the paleo-lake. It has been pointed out that diatom records from the Peloponnese are rare, due to a dry and carbonate-rich environment favoring generally alkaline conditions (Weiberg et al., 2016). Studies, conducted on the Agios Floros fen to the south and on Lake Mouria to the North-West of the Alfeios River delta, reported

TABLE 7 | Lake-level reconstruction of MAR-1.

Unit		Depth (cm)	Age (ka)	Environmental interpretation
UB1	Start	0	427	Reed belt of a seasonal anoxic lake
	End	120	434	
UB2	Start	120	434	Lake transgression
	End	150	436	
UB3	Start	150	436	Protected shallow seasonal lake/pond close to a stream;
	End	240	441	hyperconcentrated flows after meltwater influx or storm events
UB4	Start	240	441	
	End	300	444	
UB5	Start	300	444	Floodplain after meltwater input with desiccation at the end
	End	340	445	
UB6	Start	340	445	Floodplain after meltwater input with desiccation at the end
	End	385	448	
UB7	Start	385	448	Lake-deltaic environment
	End	475	454	
UB8	Start	475	454	Transition phase from shallow lake to deltaic environment
	End	510	457	
UB9	Start	510	457	Mudflow breaches the reed belt and the lake regression
	End	575	461	
UB10	Start	575	461	Anoxic lake in close proximity to a reed belt
	End	600	463	

highly alkaline waters (pH>9) resulting from the weathering of the surrounding rocks, which most likely contributed to the dissolution of the diatoms (Chatziapostolou et al., 2013; Katrantsiotis et al., 2016). Apart from the occasional diatom presence, sponge spicules are abundant throughout the investigated sequences. Experiments demonstrate that diatoms dissolve much faster than sponge spicules in alkaline environments, because of the latter's smaller surface area in relation to their size compared to diatoms, which decreases the dissolution rate pronouncedly (Conley and Schelske, 2002). An additional cause for the presence of sponge spicules in the absence of diatoms might be that the spicules may act as a sink for Si, which is a highly important constituent of the water body for diatoms (Chu et al., 2011; Maldonado et al., 2019), due to their slow dissolving behavior. The ratio Na/Ti can be used to reconstruct chemical weathering (Nesbitt and Wilson, 1992) and seems to reflect lake-internal dissolution processes due to alkalinity changes, and thus supports our conclusion. The same can also be observed for Mg/Ti and Si/Ti.

Shoreline Reconstructions of Paleo-Lake Marathousa

The sedimentation of **UB10** (>463–461 ka), described by Karkanas et al. (2018) as black clays, took place in a stable shallow, anoxic lake environment in close proximity to a reed belt, which is indicated by high TOC, low Mn/Fe, the absence of microfossils and a high C/N of 25, indicative for plants such as reeds (e.g., Meyers and Teranes, 2001; **Table 6**; **Table 7**; **Figure 3**; **Figure 5**). The reed belt itself filtered out larger sediment particles from inflowing streams, only allowing clayey particles, most likely already high in decomposed OM, to reach the study area (**Figure 7**). According to PC1-3, the alkalinity of the paleo-lake is low, lake-internal processes dominate with high productivity causing anoxic conditions of the lake waters, which prevent organisms like ostracods to thrive. Such conditions imply a warm and humid climate. Sediments like those encountered in UB10 are also called freshwater sapropel or gyttja (Stankevica et al., 2016).

The dark grey, clayey sands of **UB9** (~461–457 ka) show an initial increase in grain sizes, alkalinity, and lake oxygenation, which could be indicative of a single or multiple mass movement events (e.g., hyperconcentrated flow, Karkanas et al., 2018) that could have destroyed the reed belt (**Figure 3**, **Figure 5**, **Figure 7**). Hyperconcentrated flows often occur during first runoff events in a rainy season, intense rainstorms, lake-breakout floods or glacier-outburst floods (Pierson, 2005). The increase in precipitation (Rb/Sr) and terrestrial input (PC1) point towards a short phase of enhanced runoff, and the pronounced decrease of TOC and C/N suggests that the reed belt was not re-established, most likely due to a falling lake level. This is supported by PC2, which shows medium high pH conditions after the hyperconcentrated flow event. The change from oxic at the base to medium oxic conditions throughout UB9 is indicated by Mn/Fe and PC3. Additionally, the dark grey sediment color suggests that the runoff event was probably only a short-term event of moister conditions. The presence of sponges, which are organisms that swiftly settle in new environments (Cohen, 2003; medium alkaline conditions Si/Ti, Na/Ti, Mg/Ti), might also indicate a shift towards more favorable lake conditions, but not stable enough to allow ostracods to thrive yet.

The silts and fine sands of **UB8** (~457–454 ka), were deposited within a well oxygenated lake (Mn/Fe, PC3) that gradually regressed from UB9 most likely due to a gradual decline in moisture availability (low Rb/Sr) (**Figure 3**, **Figure 5**, **Figure 7**). A trend towards more aridity is also indicated by a decrease in terrestrial input with a shift towards internal sedimentation processes (PC1), which is supported by an increase in alkalinity and very low TOC values. Silts, sands and high amounts of shell fragments and high TIC, suggest an

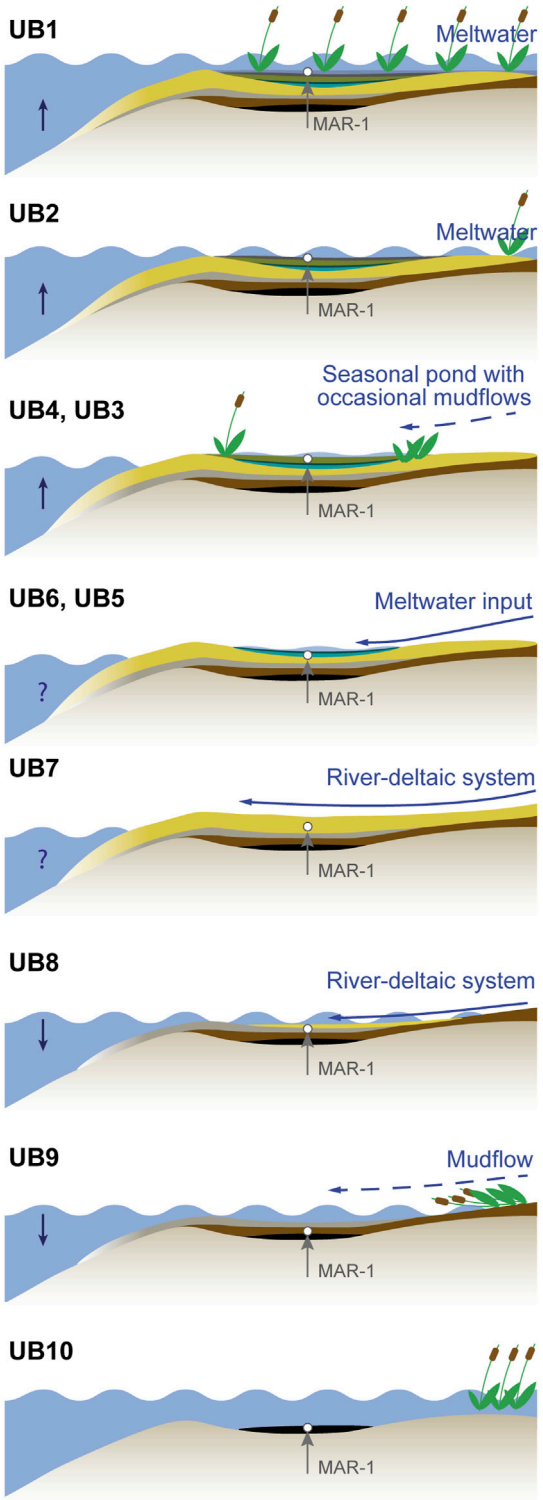

FIGURE 7 | Schematic overview of the sedimentation history of MAR-1 (not to scale).

environment with alternating transport energy, which is indicative for a riverine environment and implies a shift to such conditions at the end of UB8.

The massive, yellowish, bedded silts and fine sands of **UB7** (~454–448 ka) represent a high-energy and unstable riverine-deltaic environment (**Figure 3**, **Figure 5**, **Figure 7**). Strongly fluctuating C/N (mostly terrestrial plant input) and grain sizes could reflect a periodically high and low-energy environment which is known from seasonally controlled deltaic environments. Reduced moisture availability, preventing a full lake to develop, is also indicated by low Rb/Sr and high alkalinity. An increased current velocity and a fluctuating water table with high oxygenation (Mn/Fe, PC3) prevent the deposition of organisms *in situ* as indicated by fragments of fish bones, gastropods and ostracods, which is also supported by low TIC values. A few valves of the freshwater species *Psychrodromus* sp. (lower UB7) and *P. zschokkei* (lower-middle of UB7) indicate water temperatures below 18°C (summer temperature) (Meisch, 2000). The strong coloring of the valves implies that they were transported from nearby freshwater environments (e.g., pools). The transition from UB7 to UB6 is sharp and seems to interrupt all proxies in their trends. A slight increase of Rb/Sr towards the top of UB7 indicates higher moisture availabilities, which may predict the change of the deposition regime as reflected by UB6.

The blue sandy clay of **UB6** (~448–445 ka) may be interpreted as flood plain deposits caused by large amounts of meltwater from retreating glaciers as a result of a short warm period during MIS12 (**Figure 3**, **Figure 5**, **Figure 7**). Meltwater events are suggested based on evidence at Mt. Chelmos on the Peloponnese where glaciers reached their maximum extent during MIS12 (Leontaritis et al., 2020). During the previous arid phase between upper UB8 and most of UB7, large amounts of Saharan dust, reflected by La (e.g., Muhs et al., 2010; Varga et al., 2014) have been incorporated in the surrounding glaciers. With the onset of the brief warming phase after Heinrich-type event 6 (H_{t6}), at the transition from UB7 to UB6, large volumes of meltwater from retreating glaciers may have introduced their sediment load (mostly very fine-grained material) into the Megalopolis Basin and caused the pronounced peak of La. UB6 can be divided into two subunits. The lower UB6 is characterized by the dominance of grain sizes <63 μm, a sudden drop in alkalinity, oxic water conditions, and high terrestrial sediment input. Despite the pronounced increase in terrestrial material, C/N ratios drop, which could be indicative for a low energy environment at MAR-1 and could explain the higher abundance of diatom and sponge spicules (also observed by Field et al., 2018) in the sediments. Diatom assemblages are dominated by benthic taxa indicating shallow, but nutrient rich water conditions at MAR-1 (Field et al., 2018). Furthermore, a lack of terrestrial vegetation as indicated by low C/N ratios could support the hypothesis of meltwater as the source for the sediments of lower UB6. The upper part of the UB6 sediments reflect a shallow lake with increasing alkalinity, temporarily low oxygenation and predominating lake-internal processes. This interpretation is supported by the reduction in diatom abundances, as reported also by Field et al. (2018). However, in contrast to their interpretation of the development of a deeper lake environment based on the (relatively low) abundance of mainly planktonic diatoms such as *Aulacoseira* spp., we suggest lower water levels. The abundance of these particular species

could be due to taphonomic reasons, as *Aulacoseira* spp. consists of thick silicate valves, which dissolve slowly. Additionally, if light penetration is reduced due to, for example, organic-rich or muddy waters, only planktonic species can thrive. Higher grain sizes and higher C/N ratios at the upper part of UB6 indicate that the shoreline of this shallow paleo-lake is not far. UB6 ends with mud cracks (Karkanas et al., 2018), suggesting a desiccation of the shallow lake, in agreement with Field et al. (2018), who inferred a warmer and drier climate based on Chloridoid grass phytoliths analysis.

The proxies of the dark grey, organic-rich muddy and silty sands of **UB5** (~445–444 ka), as described by Karkanas et al. (2018), resemble those from lower UB6, with a slight reduction in their absolute values. One exception is marked by Rb/Sr, a proxy for humidity, which is more enhanced than in lower UB6. Based on the congruence of all chemical, physical and biological proxies, we infer a similar deposition history, with an increased meltwater event that flooded MAR-1 and partly eroded the underlying upper UB6 in some areas of the Marathousa 1 site (**Figure 3**, **Figure 5**, **Figure 7**). UB5 ends with another desiccation event, which is indicated by mud cracks at the upper boundary to UB4 (Karkanas et al., 2018). Such recurring droughts are consistent with findings by Field et al. (2018).

The proxies of the dark grey, organic-rich muddy sands of **UB4** (~444–441 ka) suggest the existence of a freshwater pond close to a small river or stream at MAR-1, that was periodically flooded (**Figure 3**, **Figure 5**, **Figure 7**). Locally distributed intraclasts and fining upward trends indicate multiple hyperconcentrated flows that reached the depositional area (Karkanas et al., 2018). The sequence shows conditions that allowed a number of microorganisms to thrive, including a diversity of ostracods, in contrast to the previous units. The ostracod species *Neglecandona altoides* and *Candona neglecta* (both deposited *in situ*), *Pseudocandona* cf. *marchica*, *Ilyocypris gibba* and *Prionocypris zenkeri* at the base of UB4 indicate the existence of a shallow freshwater pond of max. 10.5°C and low salinity ranges between 0 and 5% with a swampy vegetation nearby (Wagner, 1957; Devoto, 1965; De Decker, 1979; Meisch and Wouters, 2004; Fuhrmann, 2012). These paleo-environmental settings are also supported by enhanced C/N values, benthic diatom abundances (Field et al., 2018) and medium to low alkalinity. Towards the middle of UB4, increasing grain sizes, alkalinity and the lack of ostracod juveniles, as well as the monospecific abundance of *N. altoides* indicate a rather stressful environment for ostracods, with a change towards a more seasonal water body (Fuhrmann, 2012). It is difficult to tell whether the cause for these abrupt changes was a slight reduction in precipitation (Rb/Sr), a short-term event such as seasonally-induced hyperconcentrated flows (Karkanas et al., 2018), or a tectonic event. In any case, the archeological horizon of MAR-1 is situated in this lower part of UB4. Giusti et al. (2018) have reported that the site was subjected to minor post-depositional reworking processes such as those of mass movement events (e.g., mudflows), which would agree with the findings of our paleo-environmental interpretation. Towards the top of UB4, the ostracod numbers increase again, however the species domination changed towards *Ilyocypris bradyi* and *I. getica,* now indicating the steady existence of a slowly flowing stream or spring of 10–15°C (Fuhrmann, 2012). We interpret these temperatures as mean summer temperatures, in agreement with Hughes et al. (2007), who postulated that the MIS12 was characterized by summer temperatures at least 11°C colder than those observed in present-day Greece. This would imply mean summer temperatures for the Megalopolis Basin of around 10.5°C compared to today's 21.5°C. Hughes et al. (2007) also noted that mean winter temperatures were at least −0.8°C, suggesting that the water bodies may have been frozen, providing poor habitat conditions for ostracods. Furthermore, a freshwater to oligohaline vegetated pond or swamp with water temperatures ranging from 10 to 15°C can be deduced also for the archeological and *Palaeoloxodon*-bearing unit UA3 of Area A (stratigraphically correlated with UB4; Karkanas et al., 2018). In particular, in its base (UA3c), *Candona* spp. (juveniles) are recorded, while towards its middle (UA3b) ostracods increase in number and diversity, and include *Sarscypridopsis* sp., *Ilyocypris gibba* and *I. getica*; at its top (UA3a) again only juveniles of *Candona* spp. are identified. Overall, for UA3, the taphonomic indices reveal relatively high transportation rates of juvenile valves from a small stream.

The dark grey, organic-rich muddy sands of **UB3** (~441–436 ka) resemble those of UB4 and many proxies continue their indicated trends (**Figure 3**, **Figure 5**, **Figure 7**). The return of the ostracod species *Neglecandona altoides* and persistence throughout UB3, suggests the existence of a more or less permanent, but small water body. Based on the appearance of *Psychrodromus* sp., *Ilyocypris getica* and *I. decipiens,* the water body was ~15°C with low salinity values. Disturbed sediments, most likely affected by hyperconcentrated flows (Karkanas et al., 2018) after meltwater pulses or storm events, are confirmed by the taphonomy of ostracods, which indicate disturbed sediment-water interfaces and transported valves throughout this unit. The small pond or stream (when present) was well oxygenated and of low alkalinity, allowing sponges and diatoms to thrive and be better preserved. Our observations confirm Field et al. (2018), who also inferred a shallow water body based on carpological assemblages and unsorted wood remains. Furthermore, it might be possible that a reed belt nearby was reestablished based on an increased amount of reed phytoliths in the sediments and the enhanced C/N ratios (~20). Towards the top of UB3 environmental conditions change and the water body becomes less oxygenated, which might have caused the ostracods to disappear. A possible enhanced precipitation (Rb/Sr) and associated higher input of terrestrial material (Ti, PC1) may have contributed more nutrients and water to a system where high productivity might have caused anoxia at some point.

The dark grey, organic-rich silty sands of **UB2** (~436–434 ka) with their high concentrations of shells and shell fragments can be attributed to a high-energy environment associated with a rising lake level (**Figure 3**, **Figure 5**, **Figure 7**). Such winnowed shell bars at or above the wave base, together with higher grain sizes, are common features of storm events (Cohen, 2003). The high number of shell fragments is also reflected by the microfossil record, where gastropods and opercula are dominating together with enhanced grain sizes. The absence of ostracods supports the

high energy environment hypothesis, since the light and fragile valves are easily transported or destroyed. However, there is no evidence that the high energy environment was a constant state at this stage of the lake development.

The black sandy to clayey lignite of **UB1** (<434–427 ka) was deposited in a shallow body of standing water inside a reed belt (**Figure 3**, **Figure 5**, **Figure 7**) as indicated by high TOC, high C/N. The location of sedimentation is expected to be closer to margins of the water body, as indicated by high grain sizes, which stands in contrast to UB10, where high grain sizes were filtered out since the site was located most likely in front of the reed belt further away from the lake margin (Valero-Garcés et al., 2014). The degradation of the OM leads to anoxic conditions (Mn/Fe), which is supported by the absence of aquatic microfossils and the good preservation of plant material (Field et al., 2018). The increase in the number of leaves and wood found by Field et al. (2018) points towards the end of the previous dry conditions (UB8-UB3).

The Local Impact of Global Climate Change

The sedimentary sequence of MAR-1 was deposited during the glacial MIS12 (480–420 ka), which is known as the Skamnellian Stage in the glacial sequence of Greece (Leontaritis et al., 2020). During MIS12, the global sea level fell by ~100 m (Spratt and Lisiecki, 2016). From the N-Atlantic viewpoint, MIS12 is described as an unstable glacial, that was bounded on both ends by the stable interglacials MIS13 and MIS11 (**Figure 1**; **Figure 7**; e.g., McManus et al., 1999; Stein et al., 2009; Rodrigues et al., 2011; Regattieri et al., 2016). Terrestrial records of the Mediterranean region depict the glacial of MIS12 as generally cold and dry with a noticeable advance of glaciers (e.g., Tzedakis et al., 2006; Francke et al., 2016; Regattieri et al., 2016; Villa et al., 2016; Koutsodendris et al., 2019). There is evidence in Greece that the glaciers on Mt. Tymphi (N-Greece), Mt. Smolikas (N-Greece) and Mt. Chelmos (Peloponnese) reached their maximum extent during that time (Leontaritis et al., 2020).

In the Megalopolis Basin, the initial phase (**UB10**) >463–461 ka of the investigated sediment sequence is characterized by a reed-fringed, probably shallow, anoxic lake that formed during a humid and warm climate (**Figure 7**). Within the limits of the respective age models, such warmer and humid conditions at the beginning of MIS12 have also been reported from Lake Ohrid (Albania-North Macedonia), the Sulmona Basin (Italy), Tenaghi Philippon (NE Greece) and the southern Megalopolis Basin (**Figure 1**, **Figure 8**; e.g., Okuda et al., 2002; Tzedakis et al., 2006; Francke et al., 2016; Regattieri et al., 2016; Villa et al., 2016; Koutsodendris et al., 2019; Wagner et al., 2019). The Mediterranean sea surface temperatures (SST), however, remained low although slightly increasing, while the reported N-Atlantic SSTs are declining towards UB9 (Wang et al., 2010; Alonso-Garcia et al., 2011).

The sediments of **UB9** (~461–457 ka) reflect a mass movement event that might have been caused by a short but intense increase in precipitation and associated short-term freshwater lake conditions (**Figure 7**). The Mediterranean and the N-Atlantic show contrasting SSTs, which are however, slightly increasing towards the top of UB9 (**Figure 8**; Wang et al., 2010; Alonso-Garcia et al., 2011). Continuing warm conditions are reported from bulk carbonates $\delta^{18}O$ composition of the Sulmona Basin (Regattieri et al., 2016; Villa et al., 2016). Pollen obtained from sediments at Lake Ohrid (Albania, North Macedonia), Tenaghi Philippon (NE Greece) and the Megalopolis Basin reflect a highly fluctuating moisture availability with a decreasing trend (Okuda et al., 2002; Tzedakis et al., 2006; Koutsodendris et al., 2019). The simulated (LOVECLIM) precipitation evolution at Lake Ohrid by Wagner et al. (2019), however, shows no fluctuations, in contrast to its pollen record, but the authors state that the model tends to underestimate short-term precipitation changes. Such contrasting climatic conditions as indicated from the land and sea records could be an explanation for the short-term precipitation increase and associated mudflow. Kwiecien et al. (2009) stated that SSTs are a major factor in the cyclogenesis of the Mediterranean, with storms forming when temperature gradients are steepest, which occurs more frequently during intense winters today. Such contrasting SST conditions during a glacial could have generated increased storminess and the associated enhanced short-term precipitation in the Mediterranean. Such conditions could have existed at the time of UB9 deposition and could have been a precursor for a prolonged cold and dry period which is presented by UB8 and UB7.

UB8 deposition (~457–454 ka) occurred most likely during a time of progressive aridification that caused MAR-1 to turn from a shallow lake into a deltaic environment by the upper end of UB8 (**Figure 7**). A pronounced decrease in mean annual temperatures and precipitation is also recorded in the different proxy records of the surrounding Mediterranean such as the Sulmona Basin, Lake Ohrid, Tenaghi Philippon and the Megalopolis Basin, which parallel SST declines in the N-Atlantic and Mediterranean Sea itself (Tzedakis et al., 2006; Wang et al., 2010; Alonso-Garcia et al., 2011; Regattieri et al., 2016; Koutsodendris et al., 2019; Wagner et al., 2019).

During the episode between ~454 and 448 ka (**UB7**), the riverine-lake deltaic system, which had already developed during the final stages of UB8, continued the deposition of fine sands under drier climatic conditions (**Figure 3**, **Figure 5**, **Figure 7**). A dominating grassy landscape, indicative for drier and also colder temperatures is supported by a pollen record from the Megalopolis Basin by Okuda et al. (2002). The continuation of the dry and cold period occurred over the central and eastern Mediterranean region (Okuda et al., 2002; Tzedakis et al., 2006; Regattieri et al., 2016; Koutsodendris et al., 2019; Wagner et al., 2019). Also, the marine proxies describe colder SSTs in the N-Atlantic and Western Mediterranean (**Figure 8**; Wang et al., 2010; Alonso-Garcia et al., 2011). Towards the top of the UB7 sequence, however, a warming in the marine records is reported, which falls into a time period where slightly enhanced precipitation and temperatures at Lake Ohrid and the Megalopolis Basin are suggested by pollen assemblages. Tenaghi Philippon, however, seems to have remained dry and cold according to the arboreal pollen record of (Tzedakis et al. 2006), although this could be a

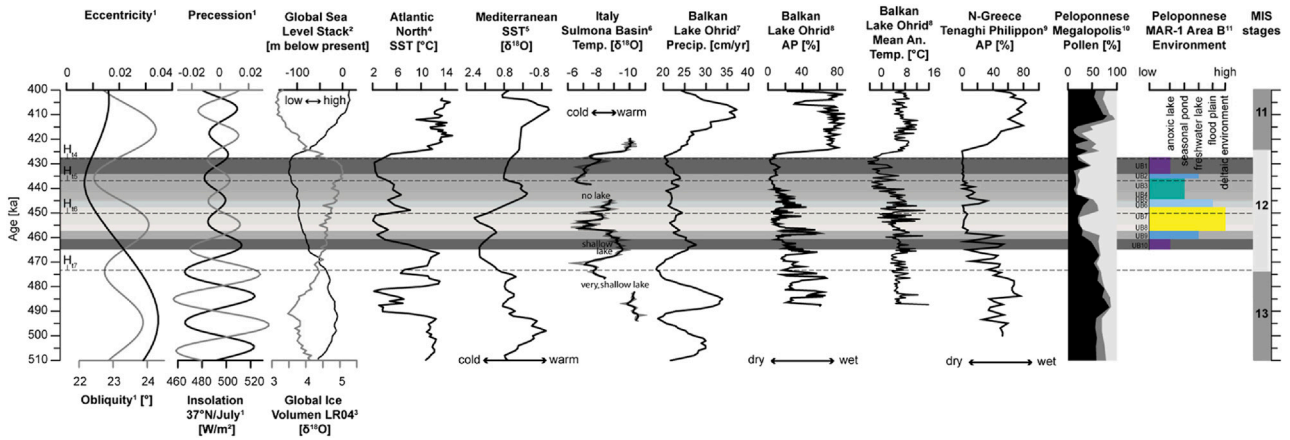

FIGURE 8 | Global records compared to the paleoenvironmental interpretation of MAR-1. 1) Orbital parameters and the local (37°N) mean monthly insolation (21. June–20. July; Laskar et al., 2004). 2) Stacked global sea level curve (Spratt and Lisiecki, 2016). 3) Global ice volume based on the benthic isotope stack LR04 (Lisiecki and Raymo, 2005). 4) Mean annual SST based on planktonic foraminifera, N-Atlantic (Alonso-Garcia et al., 2011). 5) Mediterranean SST based on the $\delta^{18}O$ stack of the planktonic foraminifera *Globigerinoides ruber* (Wang et al., 2010). 6) $\delta^{18}O$ record from the Sulmona Basin, Italy (Regattieri et al., 2016). 7) Calculated precipitation model (LOVECLIM) from Lake Ohrid, Albania, North Macedonia (Wagner et al., 2019). 8) Arboreal pollen record from Lake Ohrid (Koutsodenris et al., 2019). 9) Arboreal pollen record from Tenaghi Philippon, N. Greece (Tzedakis et al., 2006). 10) Pollen record from the Megalopolis Basin, Peloponnese [black: arboreal pollen (AP); dark grey: Gramineae; bright grey: non-arboreal pollen (NAP); Okuda et al., 2002]. 11) Reconstructed paleoenvironment and lake level at MAR-1 Area B, Peloponnese (this study). The dashed line marks Heinrich-type events (H_t; Rodrigues et al., 2011). The colored shadings indicate the lithological units of MAR-1.

result of sampling resolution, the continental character of the basin and/or age-model limitations. The recorded warming and slight increase in precipitation fall into the Heinrich-type event 6 (H_{t6}) ca. 450 ka ago (Rodrigues et al., 2011).

The sediments and proxies of **UB6** (~448–445 ka) and **UB5** (~445–444 ka) indicate a warming event that may have caused a pronounced melting of the surrounding glaciers. The warming trend that started already in upper UB7 continues its trend at Sulmona Basin (Regattieri et al., 2016) and reaches one of the highest values within MIS12. Pollen records at different Mediterranean sites surrounding MAR-1 all show a continuation of the increase in arboreal taxa indicating a short-term improvement in climate (Okuda et al., 2002; Tzedakis et al., 2006; Koutsodendris et al., 2019; Wagner et al., 2019). N-Atlantic SSTs decline during UB6 and UB5, whereas western Mediterranean SSTs continue the warming trend which could have caused an enhanced storminess during this time, due to potential strong temperature gradients (Kwiecien et al., 2009; Wang et al., 2010; Alonso-Garcia et al., 2011).

The proxies of **UB4** (contains archaeological remains) to **UB3** (~444–436 ka) indicate the existence of a seasonal pond or slow flowing stream that became stagnant and anoxic in the very upper part of UB3. The water temperatures, as inferred from ostracod assemblages, were cold and ranged from 10 to 15°C. Precipitation (Rb/Sr, PC2) was low during these episodes and only slightly increased towards the top of UB3. A strong reduction towards colder temperatures is also reported from the Sulmona Basin and Lake Ohrid (Regattieri et al., 2016; Koutsodendris et al., 2019). Pollen records from Lake Ohrid, Tenaghi Philippon and Megalopolis report taxa that reflect a rather cold and dry climate (Okuda et al., 2002; Tzedakis et al., 2006; Koutsodendris et al., 2019). The simulated (LOVECLIM) precipitation evolution at Lake Ohrid by Wagner et al. (2019) also reports reduced moisture conditions whereas Mediterranean SSTs reached highest values whereas the N-Atlantic continues its cooling trend (Wang et al., 2010; Alonso-Garcia et al., 2011).

The upper units **UB2-UB1** (~436–427 ka) of MAR-1 have been deposited in a swamp-like environment, reflecting a permanent stagnating anoxic water body. According to the Rb/Sr and PC2 records, precipitation was low, which concurs with other terrestrial proxies around the central and eastern Mediterranean (Tzedakis et al., 2006; Koutsodendris et al., 2019; Wagner et al., 2019) and is similar to conditions during UB8 and UB7. An increase in temperature is recorded in the $\delta^{18}O$ record from the Sulmona Basin (Regattieri et al., 2016). The N-Atlantic during this time continues its cooling trend and records temperatures as low as during UB8 and UB7 (Alonso-Garcia et al., 2011). The Mediterranean SSTs, in contrast, remain high despite a short cooling trend during UB3, and increases gradually towards MIS11 (Wang et al., 2010). Despite the dry conditions, the slow warming of the Mediterranean realm might have progressively forced the retreat of the widespread glaciers at the end of MIS12 (Leontaritis et al., 2020). The local increase in moisture availability, for example as soil moisture, due to melting glaciers in the catchment, might also explain the abundance of arboreal pollen in the Megalopolis pollen record (Okuda et al., 2002), whereas other regions remained free of arboreal pollen. This hypothesis is supported by the reversed cooling trend of the Mediterranean SST record. The stacked Mediterranean $\delta^{18}O$ record, based on the planktonic foraminifera *Globigerinoides ruber,* registers a slow but gradual warming. The turn towards lighter values during this time might be associated with freshwater lenses, floating on top of highly saline subsurface waters (Lourens, 2004; Wang et al., 2010). Such freshwater

lenses could indicate an increase of terrestrial runoff due to glacier retreat at the end of MIS12 and/or increased precipitation. Studies conducted on similar settings like MAR-1 suggest that mires, which lead to the formation of lignites, usually form in the warm climate of an interglacial (e.g., Mädler, 1971; Nickel et al., 1996; van Vugt et al., 2000; Okuda et al., 2002; Siavalas et al., 2009). Here we suggest that UB1 is representing the transition from the MIS12 glacial to MIS11 interglacial.

SUMMARY AND CONCLUSION

The fluvio-lacustrine sediments in the Megalopolis Basin (central Peloponnese) close to the elephant-butchering site MAR-1 were investigated to a) reconstruct the water level history in relation to the archeological site, b) refine the age model for a better disentangling of the local impact of global climate changes and c) determine the potential as a refugium for hominins during the MIS12 glacial. A multiproxy approach considering ostracods, sponge spicules, diatoms, grain sizes, TC-TN-TOC, and conventional XRF analysis provided a detailed paleoenvironmental picture during MIS12 of each identified sedimentary unit. Between ~463 and 461 ka (UB10), a reed-fringed, stable, but anoxic lake dried up gradually with the onset of drier and colder conditions of the MIS12 glacial period. A short, but intense increase in precipitation caused a return to fresh-water conditions between ~461 and 457 ka (UB9), before MAR-1 turned into a riverine environment under the progressive aridification of the region between ~457 and 448 ka (UB8-UB7). A period of warming between ~448 and 444 ka (UB6-UB5) turned the study area into a flood plain, despite ongoing dry conditions. We relate the short-term increase in water availability, despite dry conditions, to an enhanced melting of the surrounding glaciers due to the warming event. Afterwards, seasonal ponds developed between 444 and 436 ka (UB4-UB3) under a mostly dry and cold climate, which persisted over ~10 ka. These aquatic environments were rich in ostracods, diatoms and other microorganisms providing food for smaller animals and thus would have also offered mammals and humans valuable resources, such as potable water, a wide range of plant species and hunting opportunities. Pond-like conditions, such as those reflected by the sediments of UB5-UB3, thus facilitate a high archeological potential. Towards the end of MIS12 ~436–427 ka (UB2–UB1), the freshwater ponds turned into an anoxic stagnant water body after wide-spread flooding due to melting glaciers in the catchment caused by warm but still dry conditions. The reconstructed paleo-environment of MAR-1 agrees well with other records from the Mediterranean realm, with a strong linkage to climate in the N-Atlantic. We conclude that the Megalopolis Basin served as a refuge region for mammals including hominins due to its capability to retain water even during dry periods within a temperature- and storm-protected basin surrounded by mountains.

DATA AVAILABILITY STATEMENT

The original contributions presented in the study are included in the article/Supplementary Material, further inquiries can be directed to the corresponding author.

AUTHOR CONTRIBUTIONS

The study was designed by AJ. IB, AJ, NT, VT, and GK collected samples. IB and AJ developed the age model, performed statistical analysis and overall interpretation of the multiproxy record. MW, ES, and CZ conducted TOC, TIC, XRF, grain sizes, sponge and diatom analysis. PP and GI performed ostracod analysis. VT, GK, PK, NT, SK, EP, and KH contributed data from the Megalopolis Basin. All co-authors contributed to writing, refining and approving the manuscript.

FUNDING

The research has been funded by the European Research Council (ERC StG 283503 "Paleoanthropology at the Gates of Europe" and ERC CoG 724703, "Human evolution at the crossroads", awarded to KH), the Senckenberg Centre for Human Evolution and Paleoenvironment (S-HEP) in Tübingen and the Open Access Publishing Fund of the University of Tübingen.

ACKNOWLEDGMENTS

This research was conducted under the auspices of the Ephoreia of Paleoanthropology and Speleology, Greek Ministry of Culture, and was supported by the European Research Council (PaGE, CROSSROADS awarded to KH). We thank the Senckenberg Centre for Human Evolution and Paleoenvironment (S-HEP) in Tübingen for funding the doctoral project of IB. We greatly thank Tatiana Miranda for her constant laboratory support and advice, H. Taubald for assisting with XRF measurements/data and S. Fleiz for support in TOC and TIC analysis at Tübingen university. We thank both reviewers for their constructive comments that helped increasing the quality of the manuscript.

REFERENCES

Abdi, H., and Williams, L. J. (2010). Principal Component Analysis. *Wires Comp. Stat.* 2 (4), 433–459. doi:10.1002/wics.101

Alonso-Garcia, M., Sierro, F. J., and Flores, J. A. (2011). Arctic Front Shifts in the Subpolar North Atlantic during the Mid-pleistocene (800-400ka) and Their Implications for Ocean Circulation. *Palaeogeogr. Palaeoclimatol. Palaeoecol.* 311 (3–4), 268–280. doi:10.1016/j.palaeo.2011.09.004

Athersuch, J. (1976). Stereo-Atlas Ostracod Shells 3 (21), 117–124.

Athersuch, J., Bate, R. H., Boomer, I. D., Horne, D. J., Lord, A. R., Neale, J. W., et al. (1973–1996). *A Stereoatlas of Ostracod Shells. Several Volumes*. British Micropalaeontological Society.

Baltatzis, E. G., and Katagas, C. G. (1984). The Pumpellyite-Actinolite and Contiguous Facies in Part of the Phyllite-Quartzite Series, central Northern

Peloponnesus, Greece. *J. Metamorph Geol.* 2 (4), 349–363. doi:10.1111/j.1525-1314.1984.tb00595.x

Battarbee, R. W., (1986). Diatom Analysis. In: *Handbook of Holocene Palaeoecology and Palaeohydrology*, ed. by Björn. E. Berglund. Wiley, Chichester, pp. 527–570. ISBN 0-471-90691-3.

Belis, C. A. (1997). Palaeoenvironmental Reconstruction of Lago di Albano (Central Italy) during the Late Pleistocene using fossil ostracod assemblages. *Water Air Soil Pollut.* 99 (1–4), 593–600. doi:10.1007/BF02406898

Bhattacharya, B., and Habtzghi, D. (2002). Median of thepValue under the Alternative Hypothesis. *The Am. Statistician* 56 (3), 202–206. doi:10.1198/000313002146

Bishop, J. K. B. (1988). The Barite-Opal-Organic Carbon Association in Oceanic Particulate Matter. *Nature* 332, 341–343. doi:10.1038/332341a0

Blaauw, M., and Christen, J. A. (2011). Flexible Paleoclimate Age-Depth Models Using an Autoregressive Gamma Process. *Bayesian Anal.* 6 (3), 457–474. doi:10.1214/ba/1339616472

Blackwell, B. A. B., Sakhrani, N., Singh, I. K., Gopalkrishna, K. K., Tourloukis, V., Panagopoulou, E., et al. (2018). ESR Dating Ungulate Teeth and Molluscs from the Paleolithic Site Marathousa 1, Megalopolis Basin, Greece. *Quaternary* 1, 22. doi:10.3390/quat1030022

Breman, E. (1980). Differential Distribution of Left and Right Ostracode Valves in the Adriatic Sea. *Palaeogeogr. Palaeoclimatol. Palaeoecol.* 32, 135–141. doi:10.1016/0031-0182(80)90036-X

Burn, M. J., and Palmer, S. E. (2014). Solar Forcing of Caribbean Drought Events during the Last Millennium. *J. Quat. Sci.* 29, 827–836. doi:10.1002/jqs.2660

Calvert, S. E., and Pedersen, T. F. (2007). "Chapter Fourteen Elemental Proxies for Palaeoclimatic and Palaeoceanographic Variability in Marine Sediments: Interpretation and Application," in *Proxies in Late Cenozoic Paleoceanography*. Editors C. Hillaire-Marcel and A. De Vernal (Dev Mar Geol, Elsevier), 567–644. doi:10.1016/s1572-5480(07)01019-6

Chatziapostolou, A., Siavalas, G., Kalaitzidis, S., and Christanis, K. (2013). Geological Study for a Wetland Restoration: the Case of the Drained Mouria Lake (W. Peloponnese). *Geosociety* 47 (1), 72–81. doi:10.12681/bgsg.10902

Chawchai, S., Kylander, M. E., Chabangborn, A., Löwemark, L., and Wohlfarth, B. (2016). Testing Commonly Used X-Ray Fluorescence Core Scanning-Based Proxies for Organic-Rich Lake Sediments and Peat. *Boreas* 45 (1), 180–189. doi:10.1111/bor.12145

Chen, J., An, Z., Liu, L., Ji, J., Yang, J., and Chen, Y. (2001). Variations in Chemical Compositions of the Eolian Dust in Chinese Loess Plateau over the Past 2.5 Ma and Chemical Weathering in the Asian Inland. *Sci. China Ser. D-earth Sci.* 44 (5), 403–413. doi:10.1007/BF02909779

Cen, J. a., Wan, G., Zhang, D. D., Zhang, F., and Huang, R. (2004). Environmental Records of Lacustrine Sediments in Different Time Scales: Sediment Grain Size as an Example. *Sci. China Ser. D* 47, 954–960. doi:10.1360/03yd0160

Chu, J., Maldonado, M., Yahel, G., and Leys, S. (2011). Glass Sponge Reefs as a Silicon Sink. *Mar. Ecol. Prog. Ser.* 441, 1–14. doi:10.3354/meps09381

Cohen, A. S. (2003). *Paleolimnology: The History and Evolution of lake Systems*. Oxford University Press. 0-19-513353-6. doi:10.1093/oso/9780195133530.001.0001

Cole, J. M., Goldstein, S. L., deMenocal, P. B., Hemming, S. R., and Grousset, F. E. (2009). Contrasting Compositions of Saharan Dust in the Eastern Atlantic Ocean during the Last Deglaciation and African Humid Period. *Earth Planet. Sci. Lett.* 278, 257–266. doi:10.1016/j.epsl.2008.12.011

Conley, D. J., and Schelske, C. L. (2002). "Biogenic Silica," in *Tracking Environmental Change Using Lake Sediments. Developments in Paleoenvironmental Research*. Editors J. P. Smol, H. J. B. Birks, W. M. Last, R. S. Bradley, and K. Alverson, 3, 281–293. doi:10.1007/0-306-47668-1_14

Cuven, S., Francus, P., and Lamoureux, S. F. (2010). Estimation of Grain Size Variability with Micro X-ray Fluorescence in Laminated Lacustrine Sediments, Cape Bounty, Canadian High Arctic. *J. Paleolimnol.* 44 (3), 803–817. doi:10.1007/s10933-010-9453-1

Danatsas, I. (1994). Jungneogene Ostrakoden aus der NW- und N-Pelopennes (Griechenland). *Münstersche Forschungen zur Geologie and Paläontologie* 76, 97–167.

Daskalaki, P. (2002). Contribution to Chemistry and Quality of Groundwater in Greece. Unpubl. Ph.D. Thesis. Dept. of Geology, University of Patras, 947.

Davison, W. (1993). Iron and Manganese in Lakes. *Earth-Science Rev.* 34, 119–163. doi:10.1016/0012-8252(93)90029-7

Dayan, U., Heffter, J., Miller, J., and Gutman, G. (1991). Dust Intrusion Events into the Mediterranean Basin. *J. Appl. Meteorology Climatology* Vol. 30, 1185–1199. doi:10.1175/1520-0450(1991)030<1185:DIEITM>2.0.CO;2

De Decker, P. (1979). The Middle Pleistocene Ostracod Fauna of the West Runton Freshwater Bed. *Norfolk, Paleontol.* 22/2, 293–316.

Dearing, J. A. (1997). Sedimentary Indicators of lake-level Changes in the Humid Temperate Zone: a Critical Review. *J. Paleolimnology* 18, 1–14. doi:10.1023/A:1007916210820

Devoto, G. (1965). Lacustrine Pleistocene in the Lower Liri Valley. *Geologica. Romana* 4, 291–365.

Digerfeldt, G., Olsson, S., and Sandgren, P. (2000). Reconstruction of lake-level Changes in lake Xinias, central Greece, during the Last 40 000 Years. *Palaeogeogr. Palaeoclimatol. Palaeoecol.* 158 (Issues 1–2), 65–82. doi:10.1016/S0031-0182(00)00029-8

Dornsiepen, U. F., Manutsoglu, E., and Mertmann, D. (2001). Permian-Triassic Palaeogeography of the External Hellenides. *Palaeogeogr. Palaeoclimatol. Palaeoecol.* 172, 327–338. doi:10.1016/S0031-0182(01)00307-8

Doukas, C., van Kolfschoten, T., Papayianni, K., Panagopoulou, E., and Harvati, K. (2018). The Small Mammal Fauna from the Palaeolithic Site Marathousa 1 (Greece). *Quat. Int.* 497, 95–107. doi:10.1016/j.quaint.2018.09.036

Emmanouilidis, A., Katrantsiotis, C., Norström, E., Risberg, J., Kylander, M., Sheik, T. A., et al. (2018). Middle to Late Holocene Palaeoenvironmental Study of Gialova Lagoon, SW Peloponnese, Greece. *Quat. Int.* 476, 46–62. doi:10.1016/j.quaint.2018.03.005

Ermolli, E. R., Aucelli, P. P., Di Rollo, A., Mattei, M., Petrosino, P., Porreca, M., et al. (2010). An Integrated Stratigraphical Approach to the Middle Pleistocene Succession of the Sessano basin (Molise, Italy). *Quat. Int.* 225 (1), 114–127. doi:10.1016/j.quaint.2009.04.008

Fernández, M., Björck, S., Wohlfarth, B., Maidana, N. I., Unkel, I., and Van der Putten, N. (2013). Diatom assemblage changes in lacustrine sediments from Isla de los Estados, southernmost South America, in response to shifts in the southwesterly wind belt during the last deglaciation. *J. Paleolimnol.* 50, 433–446. doi:10.1007/s10933-013-9736-4

Field, M. H., Ntinou, M., Tsartsidou, G., van Berge Henegouwen, D., Risberg, J., Tourloukis, V., et al. (2018). A Palaeoenvironmental Reconstruction (Based on Palaeobotanical Data and Diatoms) of the Middle Pleistocene Elephant (*Palaeoloxodon antiquus*) Butchery Site at Marathousa, Megalopolis, Greece. *Quat. Int.* 497, 108–122. doi:10.1016/j.quaint.2018.06.014

Fitzpatrick, R. W., and Chittleborough, D. J. (2002). "Titanium and Zirconium Minerals," in *Soil Mineralogy with Environmental Applications*. Editors J. B. Dixon and D. G. Schulze. doi:10.2136/sssabookser7

Flower, R. J. (1993). "Diatom Preservation: Experiments and Observations on Dissolution and Breakage in Modern and Fossil Material," in *Twelfth International Diatom Symposium. Developments in Hydrobiology*. Editor H. van Dam, 90, 473–484. doi:10.1007/978-94-017-3622-0_48

Foerster, V., Deocampo, D. M., Asrat, A., Günter, C., Junginger, A., Krämer, K. H., et al. (2018). Towards an Understanding of Climate Proxy Formation in the Chew Bahir basin, Southern Ethiopian Rift. *Palaeogeogr. Palaeoclimatol. Palaeoecol.* 501, 111–123. doi:10.1016/j.palaeo.2018.04.009

Francke, A., Wagner, B., Just, J., Leicher, N., Gromig, R., Baumgarten, H., et al. (2016). Sedimentological Processes and Environmental Variability at Lake Ohrid (Macedonia, Albania) between 637 Ka and the Present. *Biogeosciences* 13, 1179–1196. doi:10.5194/bg-13-1179-2016

Frenzel, P., and Boomer, I. (2005). The Use of Ostracods from Marginal marine, Brackish Waters as Bioindicators of Modern and Quaternary Environmental Change. *Palaeogeogr. Palaeoclimatol. Palaeoecol.* 225, 68–92. doi:10.1016/j.palaeo.2004.02.051

Frenzel, P., Keyser, D., and Viehberg, F. A. (2010). An Illustrated Key and (Palaeo) ecological Primer for Postglacial to Recent Ostracoda (Crustacea) of the Baltic Sea. *Boreas* 39 (3), 567–575. doi:10.1111/j.1502-3885.2009.00135.x

Frogley, M. R., (1998). The Biostratigraphy, Palaeoecology and Geochemistry of a Long Lacustrine Sequence from NW Greece (Doctoral Thesis). doi:10.17863/CAM.16400

Frost, T. M., Reiswig, H. M., and Riccardi, A. (2001). "Porifera," in *Ecology and Classification of North American Freshwater Invertebrates*. Editors J. H. Thorp and A. P. Covich. 2nd Edition (Academic Press), 97–133. 9780080530673.

Fuhrmann, R. (2012). Atlas quartärer und rezenter Ostrakoden Mitteldeutschlands. *Altenburger Naturwissenschaftliche Forschungen* 15.

Giaccio, B., Leicher, N., Mannella, G., Monaco, L., Regattieri, E., Wagner, B., et al. (2019). Extending the Tephra and Palaeoenvironmental Record of the Central Mediterranean Back to 430 ka: A New Core From Fucino Basin, Central Italy. *Quat. Sci. Rev.* 225, 106003. doi:10.1016/j.quascirev.2019.106003

Giusti, D., Tourloukis, V., Konidaris, G., Thompson, N., Karkanas, P., Panagopoulou, E., et al. (2018). Beyond Maps: Patterns of Formation Processes at the Middle Pleistocene Open-Air Site of Marathousa 1, Megalopolis Basin, Greece. *Quat. Int.* 497, 137–153. doi:10.1016/j.quaint.2018.01.041

Givati, A., and Rosenfeld, D. (2013). The Arctic Oscillation, Climate Change and the Effects on Precipitation in Israel. *Atmos. Res.* 132–133 (133), 114–124. doi:10.1016/j.atmosres.2013.05.001

Grove, C. A., Nagtegaal, R., Zinke, J., Scheufen, T., Koster, B., Kasper, S., et al. (2010). River Runoff Reconstructions from Novel Spectral Luminescence Scanning of Massive Coral Skeletons. *Coral Reefs* 29, 579–591. doi:10.1007/s00338-010-0629-y

Haberzettl, T., Corbella, H., Fey, M., Janssen, S., Lucke, A., Mayr, C., et al. (2007). Lateglacial and Holocene Wet–Dry Cycles in Southern Patagonia: Chronology, Sedimentology and Geochemistry of a Lacustrine Record From Laguna Potrok Aike, Argentina. *The Holocene* 17 (3), 297–310. doi:10.1177/0959683607076437

Hammer, Ø., Harper, D. A. T., and Ryan, P. D. (2001). PAST: Paleontological Statistics Software Package for Education and Data Analysis. *Palaeontol. Electronica*. 4 (1), 9.

Harrison, F. W. W. (1988). Utilization of Freshwater Sponges in Paleolimnological Studies. *Palaeogeogr. Palaeoclimatol. Palaeoecol.* 62 (1–4), 387–397. doi:10.1016/0031-0182(88)90063-6

Harvati, K. (2016). "Paleoanthropology in Greece: Recent Findings and Interpretations," in *Paleoanthropology of the Balkans and Anatolia: Human Evolution and its Context. Vertebrate Paleobiology and Paleoanthropology Series*. Editors K. Harvati and M. Roksandic (Dordrecht: Springer), 3–14. doi:10.1007/978-94-024-0874-4_1

Harvati, K., Panagopoulou, E., and Runnels, C. (2009). The Paleoanthropology of Greece. *Evol. Anthropol.* 18, 131–143. doi:10.1002/evan.20219

K. Harvati, G. Konidaris, and V. Tourloukis (Editors) (2018). Special Issue Human Evolution at the Gates of Europe. *Quaternary International Special Issue Volume 497 Part A*, 1–240.

Harvati, K., Röding, C., Bosman, A. M., Karakostis, F. A., Grün, R., Stringer, C., et al. (2019). Apidima Cave Fossils Provide Earliest Evidence of *Homo sapiens* in Eurasia. *Nature* 571, 500–504. doi:10.1038/s41586-019-1376-z

Harvati, K. (2021). "The Hominin Fossil Record from Greece," in *The Fossil Vertebrates of Greece Vol. 1 – Basal Vertebrates, Basal Tetrapods, Afrotherians, Glires, and Primates*. Editor E. Vlachos (Cham: Springer – Nature Publishing Group), 18.

Hemming, S. (2007). Terrigenous Sediments. *Encyclopedia Quat. Sci.* 3, 1776–1785. doi:10.1016/b0-444-52747-8/00303-3

Heymann, C., Nelle, O., Dörfler, W., Zagana, H., Nowaczyk, N., Xue, J., et al. (2013). Late Glacial to Mid-holocene Palaeoclimate Development of Southern Greece Inferred from the Sediment Sequence of Lake Stymphalia (NE-Peloponnese). *Quat. Int.* 302, 42–60. doi:10.1016/j.quaint.2013.02.014

Hibbins, S. G. (2000). *Strontium and Strontium Compounds*. Kirk-Othmer Encyclopedia of Chemical Technology. doi:10.1002/0471238961.1920181508090202.a01.pub2

Hoang van, L., Clift, P. D., Schwab, A. M., Huuse, M., Nguyen, D. A., and Zhen, S. (2010). Large-scale Erosional Response of SE Asia to Monsoon Evolution Reconstructed from Sedimentary Records of the Song Hong-Yinggehai and Qiongdongnan Basins, South China Sea. *Geol. Soc. Spec. Publ.* 342, 219–244. 10.1144/SP342.13.

Hughes, P. D., Woodward, J. C., and Gibbad, P. L. (2007). Middle Pleistocene Cold Stage Climates in the Mediterranean: New Evidence from the Glacial Record. *Earth Planet. Sci. Lett.* 253 (1-2), 50–56. doi:10.1016/j.epsl.2006.10.019

Hussain, S. M., Ganesan, P., Ravi, G., Mohan, S. P., and Sridhar, S. G. D. (2007). Distribution of Ostracoda in marine and Marginal marine Habitats off Tamil Nadu and Adjoining Areas, Southern East Cost of India and Andaman Islands: Environmental Implications. *Indian J. Mar. Sci.* 36 (4), 369–377.

Jacobs, Z., Li, B., Karkanas, P., Tourloukis, V., Thompson, N., Panagopoulou, E., et al. (2018). Optical Dating of K-Feldspar Grains from Middle Pleistocene Lacustrine Sediment at Marathousa 1 (Greece). *Quat. Int.* 497, 170–177. doi:10.1016/j.quaint.2018.06.029

Jacobson, A. D., Blum, J. D., and Walter, L. M. (2002). Reconciling the Elemental and Sr Isotope Composition of Himalayan Weathering Fluxes: Insights from the Carbonate Geochemistry of Stream Waters. *Geochimica et Cosmochimica Acta* 66 (19), 3417–3429. doi:10.1016/S0016-7037(02)00951-1,

Jin, Z., Cao, J., Wu, J., and Wang, S. (2006). A Rb/Sr Record of Catchment Weathering Response to Holocene Climate Change in Inner Mongolia. *Earth Surf. Process. Landforms* 31, 285–291. doi:10.1002/esp.1243

Jolliffe, I. T., and Cadima, J. (2016). Principal Component Analysis: a Review and Recent Developments. *Phil. Trans. R. Soc. A.* 374, 20150202. doi:10.1098/rsta.2015.0202

Jouve, G., Francus, P., Lamoureux, S., Provencher-Nolet, L., Hahn, A., Haberzettl, T., et al. (2013). Microsedimentological Characterization Using Image Analysis and μ-XRF as Indicators of Sedimentary Processes and Climate Changes during Lateglacial at Laguna Potrok Aike, Santa Cruz, Argentina. *Quat. Sci. Rev.* 71, 191–204. doi:10.1016/j.quascirev.2012.06.003

Kagan, E., Stein, M., and Marco, S. (2018). Integrated Paleoseismic Chronology of the Last Glacial Lake Lisan: From Lake Margin Seismites to Deep-Lake Mass Transport Deposits. *J. Geophys. Res. Solid Earth* 123, 2806–2824. doi:10.1002/2017JB014117

Karkanas, P., Tourloukis, V., Thompson, N., Giusti, D., Panagopoulou, E., and Harvati, K. (2018). Sedimentology and Micromorphology of the Lower Palaeolithic Lakeshore Site Marathousa 1, Megalopolis Basin, Greece. *Quat. Int.* 497, 123–136. doi:10.1016/j.quaint.2018.02.037

Katrantsiotis, C., Norström, E., Holmgren, K., Risberg, J., and Skelton, A. (2016). High-resolution Environmental Reconstruction in SW Peloponnese, Greece, Covering the Last C. 6000 years: Evidence from Agios Floros Fen, Messenian plain. *The Holocene* 26 (2), 188–204. doi:10.1177/0959683615596838

Kelepertsis, A. E., and Kontis, E. (1997). Geochemical and Mineralogical Characteristics of Pleistocene Lignites and Associated Sediments of Marathousa Coal Field, Central Peloponnese, Greece. *Chin. J. Geochem.* 16, 8–19. doi:10.1007/BF02843368

Kleman, J., Borgström, I., Skelton, A., and Hall, A. (2016). Landscape Evolution and Landform Inheritance in Tectonically Active Regions: The Case of the Southwestern Peloponnese, Greece. *Z. Geomorphol.* 171–193. doi:10.1127/zfg/2016/0283

Kemp, A. L. W., Dell, C. I., and Harper, N. S. (1978). Sedimentation Rates and a Sediment Budget for Lake Superior. *J. Great Lakes Res.* 4 (3–4), 276–287. doi:10.1016/S0380-1330(78)72198-2

Koinig, K. A., Shotyk, W., Lotter, A. F., Ohlendorf, C., and Sturm, M. (2003). 9000 Years of Geochemical Evolution of Lithogenic Major and Trace Elements in the Sediment of an alpine lake – the Role of Climate, Vegetation, and Land-Use History. *J. Paleolimnology* 30, 307–320. doi:10.1023/A:1026080712312

Konidaris, G. E., Athanassiou, A., Tourloukis, V., Thompson, N., Giusti, D., Panagopoulou, E., et al. (2018). The Skeleton of a Straight-Tusked Elephant (*Palaeoloxodon antiquus*) and Other Large Mammals from the Middle Pleistocene Butchering Locality Marathousa 1 (Megalopolis Basin, Greece): Preliminary Results. *Quat. Int.* 497, 65–84. doi:10.1016/j.quaint.2017.12.001

Köppen, W. (1918). *Klassifikation der Klimate nach Temperatur, Niederschlag und Jahreslauf*. Gotha: Petermanns Geographische Mitteilungen, 64.

Koutsodendris, A., Kousis, I., Peyron, O., Wagner, B., and Pross, J. (2019). The Marine Isotope Stage 12 Pollen Record from Lake Ohrid (SE Europe): Investigating Short-Term Climate Change under Extreme Glacial Conditions. *Quat. Sci. Rev.* 221, 105873. doi:10.1016/j.quascirev.2019.105873

Kutzbach, J. E., Chen, G., Cheng, H., Edwards, R. L., and Liu, Z. (2014). Potential Role of winter Rainfall in Explaining Increased Moisture in the Mediterranean and Middle East during Periods of Maximum Orbitally-Forced Insolation Seasonality. *Clim. Dyn.* 42 (3-4), 1079–1095. doi:10.1007/s00382-013-1692-1

Kwiecien, O., Arz, H. W., Lamy, F., Plessen, B., Bahr, A., and Haug, G. H. (2009). North Atlantic Control on Precipitation Pattern in the Eastern Mediterranean/Black Sea Region during the Last Glacial. *Quat. Res.* 71 (3), 375–384. doi:10.1016/j.yqres.2008.12.004

Kylander, M. E., Ampel, L., Wohlfarth, B., and Veres, D. (2011). High-resolution X-ray Fluorescence Core Scanning Analysis of Les Echets (France) Sedimentary Sequence: New Insights from Chemical Proxies. *J. Quat. Sci.* 26, 109–117. doi:10.1002/jqs.1438

Laskar, J., Robutel, P., Joutel, F., Gastineau, M., Correia, A. C. M., and Levrard, B. (2004). A Long-Term Numerical Solution for the Insolation Quantities of the Earth. *A&A* 428 (1), 261–285. doi:10.1051/0004-6361:20041335

Lekkas, E., Danamos, G., Skourtsos, E., and Sakellariou, D. (2002). Position of the Middle Triassic Tyros Beds in the Gavrovo-Tripolis Unit (Rhodes Island, Dodecanese, Greece). *Geologica. Carpathica*. 53 (1), 37–44.

Leontaritis, A. D., Kouli, K., and Pavlopoulos, K. (2020). The Glacial History of Greece: a Comprehensive Review. *Med. Geosc. Rev.* 2 (2), 65–90. doi:10.1007/s42990-020-00021-w

Lisiecki, L. E., and Raymo, M. E. (2005). A Pliocene-Pleistocene Stack of 57 Globally Distributed Benthic δ18O Records. *Paleoceanography* 20, a–n. doi:10.1029/2004PA001071

Liu, X., Vandenberghe, J., An, Z., Li, Y., Jin, Z., Dong, J., et al. (2016). Grain Size of Lake Qinghai Sediments: Implications for Riverine Input and Holocene Monsoon Variability. *Palaeogeogr. Palaeoclimatol. Palaeoecol.* 449, 41–51. doi:10.1016/j.palaeo.2016.02.005

Longman, J., Veres, D., and Wennrich, V. (2019). Utilisation of XRF Core Scanning on Peat and Other Highly Organic Sediments. *Quat. Int.* 514, 85–96. doi:10.1016/j.quaint.2018.10.015

Lourens, L. J. (2004). Revised Tuning of Ocean Drilling Program Site 964 and KC01B (Mediterranean) and Implications for the $\delta^{18}O$, Tephra, Calcareous Nannofossil, and Geomagnetic Reversal Chronologies of the Past 1.1 Myr. *Paleoceanography* 19, a–n. doi:10.1029/2003PA000997

Lüttig, G. (1968). Die Ostrakoden des Megalopolis-Beckens (Peloponnes) und die Grenze Tertiär/Quartär. *Giornale die Geologia* 35, 73–82.

Lüttig, G., and Marinos, G. (1962). Zur Geologie der neuen griechischen Braunkohlen-Lagerstätte von Megalopolis. *Braunk. Wärm. Energ.* 14, 222–231.

Mädler, K. (1971). Die Früchte und Samen aus der frühpleistozänen Braunkohle von Megalopolis in Griechenland und ihre ökologische Bedeutung. *Beihefte zum Geologischen Jahrbuch* 110, 1–79.

Mahowald, N. M., Muhs, D. R., Levis, S., Rasch, P. J., Yoshioka, M., Zender, C. S., et al. (2006). Change in Atmospheric mineral Aerosols in Response to Climate: Last Glacial Period, Preindustrial, Modern, and Doubled Carbon Dioxide Climates. *J. Geophys. Res.* 111, a–n. doi:10.1029/2005JD006653

Maldonado, M., López-Acosta, M., Sitjà, C., García-Puig, M., Galobart, C., Ercilla, G., et al. (2019). Sponge Skeletons as an Important Sink of Silicon in the Global Oceans. *Nat. Geosci.* 12, 815–822. doi:10.1038/s41561-019-0430-7

Manariotis, I. D., and Yannopoulos, P. C. (2014). Impact of Human Activities and Infrastructure Works on Hydro Morphological Characteristics of Alfeios River, Greece. *Glob. NEST J.* 16, 136–145.

Mannella, G., Giaccio, B., Zanchetta, G., Regattieri, E., Niespolo, E. M., Pereira, A., et al. (2019). Palaeoenvironmental and Palaeohydrological Variability of Mountain Areas in the central Mediterranean Region: A 190 Ka-Long Chronicle from the Independently Dated Fucino Palaeolake Record (central Italy). *Quat. Sci. Rev.* 210, 190–210. doi:10.1016/j.quascirev.2019.02.032

Martens, K., and Savatenalinton, S. (2011). A Subjective Checklist of the Recent, Free-Living, Non-marine Ostracoda (Crustacea). *Zootaxa* 2855, 1–79. doi:10.11646/zootaxa.2855.1.1

Mazzini, I., Gliozzi, E., Rossetti, G., and Pieri, V. (2014). The Ilyocypris Puzzle: A Multidisciplinary Approach to the Study of Phenotypic Variability. *Int. Rev. Hydrobiology* 99 (1-14). doi:10.1002/iroh.201301729

McManus, J., Berelson, W. M., Klinkhammer, G. P., Johnson, K. S., Coale, K. H., Anderson, R. F., et al. (1998). Geochemistry of Barium in marine Sediments: Implications for its Use as a Paleoproxy. *Geochimica et Cosmochimica Acta* 62, 3453–3473. doi:10.1016/s0016-7037(98)00248-8

McManus, J. F., Oppo, D. W., and Cullen, J. L. (1999). A 0.5-Million-Year Record of Millennial-Scale Climate Variability in the North Atlantic. *Science* 283 (5404), 971–975. doi:10.1126/science.283.5404.971

Meisch, C. (2000). *Freshwater Ostracoda of Western and Central Europe*. Spektrum Akademischer Verlag.

Meisch, C., Scharf, B., Fuhrmann, R., and Thiéry, A. (2019). *Neglecandona altoides* (Petkovski, 1961) Nov. Comb. And the Genus *Neglecandona* Krstić, 2006 (Crustacea, Ostracoda, Candonidae). *Bull. de la Société des naturalistes luxembourgeois* 121, 237–264.

Meisch, C., and Wouters, K. (2004). Valve Surface Structure of *Candona neglecta* Sars, 1887 (Crustacea, Ostracoda), *Studia Quaternaria*. 21, 15–18.

Meyers, P. A., and Benson, L. V. (1987). Sedimentary Biomarker and Isotopic Indicators of the Paleoclimatic History of the Walker Lake basin, Western Nevada. *Org. Geochem.* 13 (issues 4–6), 807–813. doi:10.1016/0146-6380(88)90104-0

Meyers, P. A., and Teranes, J. L. (2001). "Sediment Organic Matter," in *Tracking Environmental Change Using Lake Sediments Volume 2: Physical and Geochemical Methods*. Editors W. M. Last and J. P. Smol. ISBN 0-306-47670-3.

Michailidis, D., Konidaris, G. E., Athanassiou, A., Panagopoulou, E., and Harvati, K. (2018). The Ornithological Remains from Marathousa 1 (Middle Pleistocene; Megalopolis Basin, Greece). *Quat. Int.* 497, 85–94. doi:10.1016/j.quaint.2018.06.045

Muhs, D. R., Budahn, J., Avila, A., Skipp, G., Freeman, J., and Patterson, D. (2010). The Role of African Dust in the Formation of Quaternary Soils on Mallorca, Spain and Implications for the Genesis of Red Mediterranean Soils. *Quat. Sci. Rev.* 29 (19-20), 2518–2543. doi:10.1016/j.quascirev.2010.04.013

Muhs, D. R., Budahn, J. R., Prospero, J. M., and Carey, S. N. (2007). Geochemical Evidence for African Dust Inputs to Soils of Western Atlantic Islands: Barbados, the Bahamas, and Florida. *J. Geophys. Res.* 112, F02009. doi:10.1029/2005JF000445

Naeher, S., Gilli, A., North, R. P., Hamann, Y., and Schubert, C. J. (2013). Tracing Bottom Water Oxygenation with Sedimentary Mn/Fe Ratios in Lake Zurich, Switzerland. *Chem. Geology* 352, 125–133. doi:10.1016/j.chemgeo.2013.06.006

Nava, S., Becagli, S., Calzolai, G., Chiari, M., Lucarelli, F., Prati, P., et al. (2012). Saharan Dust Impact in central Italy: An Overview on Three Years Elemental Data Records. *Atmos. Environ.* 60, 444–452. doi:10.1016/j.atmosenv.2012.06.064

Nesbitt, H. W., and Wilson, R. E. (1992). Recent Chemical Weathering of Basalts. *Am. J. Sci.* 292 (10), 740–777. doi:10.2475/ajs.292.10.740

Nickel, B., Riegel, W., Schönherr, T., and Velitzelos, E. (1996). Environments of Coal Formation in the Pleistocene lignite at Megalopolis, Peloponnesus (Greece) - Reconstructions from Palynological and Petrological Investigations. *njgpa* 200, 201–220. doi:10.1127/njgpa/200/1996/201

Nizou, J., Hanebuth, T. J. J., and Vogt, C. (2011). Deciphering Signals of Late Holocene Fluvial and Aeolian Supply from a Shelf Sediment Depocentre off Senegal (north-west Africa). *J. Quat. Sci.* 26, 411–421. doi:10.1002/jqs.1467

Okuda, M., van Vugt, N., Nakagawa, T., Ikeya, M., Hayashida, A., Yasuda, Y., et al. (2002). Palynological Evidence for the Astronomical Origin of lignite-detritus Sequence in the Middle Pleistocene Marathousa Member, Megalopolis, SW Greece. *Earth Planet. Sci. Lett.* 201, 143–157. doi:10.1127/njgpa/200/1996/20110.1016/s0012-821x(02)00706-9

Panagopoulou, E., Tourloukis, V., Thompson, N., Athanassiou, A., Tsartsidou, G., Konidaris, G. E., et al. (2015). Marathousa 1: a New Middle Pleistocene Archaeological Site from Greece. *Antiquity* 343, 1–8.

Panagopoulou, E., Tourloukis, V., Thompson, N., Konidaris, G., Athanassiou, A., Giusti, D., et al. (2018). The Lower Palaeolithic Site of Marathousa 1, Megalopolis, Greece: Overview of the Evidence. *Quat. Int.* 497, 33–46. doi:10.1016/j.quaint.2018.06.031

Panagiotopoulos, K., Holtvoeth, J., Kouli, K., Marinova, E., Francke, A., Cvetkoska, A., et al. (2020). Insights Into the Evolution of the Young Lake Ohrid Ecosystem and Vegetation Succession From a Southern European Refugium During the Early Pleistocene. *Quat. Sci. Rev.* 227, 106044. doi:10.1016/j.quascirev.2019.106044

Papoulia, C. (2017). Seaward Dispersals to the NE Mediterranean Islands in the Pleistocene. The Lithic Evidence in Retrospect. *Quat. Int.* 431, 64–87. doi:10.1016/j.quaint.2016.02.019

Pierson, T. C. (2005). "Hyperconcentrated Flow - Transitional Process between Water Flow and Debris Flow," in *Debris-flow Hazards and Related Phenomena*. Editors M. Jakob and O. Hungr (Berlin, Heidelberg: Springer), 159–202. doi:10.1007/3-540-27129-5_8

Rantakari, M., and Kortelainen, P. (2008). Controls of Organic and Inorganic Carbon in Randomly Selected Boreal Lakes in Varied Catchments. *Biogeochemistry* 91 (2–3), 151–162. doi:10.1007/s10533-008-9266-8

Regattieri, E., Giaccio, B., Galli, P., Nomade, S., Peronace, E., Messina, P., et al. (2016). A Multi-Proxy Record of MIS 11-12 Deglaciation and Glacial MIS 12

Instability from the Sulmona basin (central Italy). *Quat. Sci. Rev.* 132, 129–145. doi:10.1016/j.quascirev.2015.11.015

Regattieri, E., Giaccio, B., Nomade, S., Francke, A., Vogel, H., Drysdale, R. N., et al. (2017). A Last Interglacial Record of Environmental Changes from the Sulmona Basin (central Italy). *Palaeogeogr. Palaeoclimatol. Palaeoecol.* 472, 51–66. doi:10.1016/j.palaeo.2017.02.013

Reiswig, H. M., Frost, T. M., and Ricciardi, A. (2010). "Porifera," in *Ecology and Classification of North American Freshwater Invertebrates*. Editors H. Thorp and A. P. Covich. Third Edition (Academic Press), 91–123. 9780123748553. doi:10.1016/B978-0-12-374855-3.00004-2

Remoundaki, E., Bourliva, A., Kokkalis, P., Mamouri, R. E., Papayannis, A., Grigoratos, T., et al. (2011). PM10 Composition during an Intense Saharan Dust Transport Event over Athens (Greece). *Sci. Total Environ.* 409 (20), 4361–4372. doi:10.1016/j.scitotenv.2011.06.026

Rodrigues, T., Voelker, A. H. L., Grimalt, J. O., Abrantes, F., and Naughton, F. (2011). Iberian Margin Sea Surface Temperature during MIS 15 to 9 (580-300 Ka): Glacial Suborbital Variability versus Interglacial Stability. *Paleoceanography* 26 (1), PA1204. doi:10.1029/2010PA001927

Rothwell, R. G., and Croudace, I. w. (2015). "Micro-XRF Studies of Sediment Cores: a Perspective on Capability and Application in the Environmental Sciences," in *Micro-XRF Studies of Sediment Cores*. Editors I. W. Croudace and R. G. Rothwell (Dordecht: Springer), 1–21. doi:10.1007/978-94-017-9849-5_1

Roy, P. D., Caballero, M., Lozano, R., and Smykatz-Kloss, W. (2008). Geochemistry of Late Quaternary Sediments from Tecocomulco lake, central Mexico: Implication to Chemical Weathering and Provenance. *Geochemistry* 68 (4), 383–393. doi:10.1016/j.chemer.2008.04.001

Ruiz, F., Abad, M., Boderat, A. M., Carbonel, P., Rodríguez-Lázaro, J., González-Regalado, M. L., et al. (2013). Freshwater Ostracods as Environmental Tracers. *Int. J. Environ. Sci. Technol.* 10, 1115–1128. doi:10.1007/s13762-013-0249-5

Schellenberg, S. A. (2007). "PALEOLIMNOLOGY | Marine Ostracods," in *Encyclopedia of Quaternary Science*. Editor S. A. Elias (Amsterdam: Elsevier), 2046–2062. doi:10.1016/b0-44-452747-8/00249-0

Shaheen, S. M., Alessi, D. S., Tack, F. M. G., Ok, Y. S., Kim, K.-H., Gustafsson, J. P., et al. (2019). Redox Chemistry of Vanadium in Soils and Sediments: Interactions with Colloidal Materials, Mobilization, Speciation, and Relevant Environmental Implications- A Review. *Adv. Colloid Interf. Sci.* 265, 1–13. doi:10.1016/j.cis.2019.01.002

Siavalas, G., Linou, M., Chatziapostolou, A., Kalaitzidis, S., Papaefthymiou, H., and Christanis, K. (2009). Palaeoenvironment of Seam I in the Marathousa Lignite Mine, Megalopolis Basin (Southern Greece). *Int. J. Coal Geology* 78 (4), 233–248. doi:10.1016/j.coal.2009.03.003

Sickenberg, O. (1975). Eine Säugetierfauna des tieferen Bihariums aus dem Becken von Megalopolis (Peleponnes, Griechenland). *Ann. Géologiques des Pays Helléniques* 27, 25–73.

Spratt, R. M., and Lisiecki, L. E. (2016). A Late Pleistocene Sea Level Stack. *Clim. Past* 12 (4), 1079–1092. doi:10.5194/cp-12-1079-2016

Stankevica, K., Vincevica-Gaile, Z., and Klavins, M. (2016). Freshwater Sapropel (Gyttja): its Description, Properties and Opportunities of Use in Contemporary Agriculture. *Agron. Res.* 14 (3), 929–947.

Stein, R., Hefter, J., Grützner, J., Voelker, A., and Naafs, B. D. A. (2009). Variability of Surface Water Characteristics and Heinrich-like Events in the Pleistocene Midlatitude North Atlantic Ocean: Biomarker and XRD Records from IODP Site U1313 (MIS 16-9). *Paleoceanography* 24, a–n. doi:10.1029/2008PA001639

Thompson, N., Tourloukis, V., Panagopoulou, E., and Harvati, K. (2018). In Search of Pleistocene Remains at the Gates of Europe: Directed Surface Survey of the Megalopolis Basin (Greece). *Quat. Int.* 497, 22–32. doi:10.1016/j.quaint.2018.03.036

Thomson, J., Croudace, I. W., and Rothwell, R. G., (2006). A Geochemical Application of the ITRAX Scanner to a Sediment Core Containing Eastern Mediterranean Sapropel Units, *Geol. Soc. Lond. Spec. Publications*. In: (ed. R. G. Rothwell) *New Techniques in Sediment Core Analysis*. 267, pp. 65–77. doi:10.1144/GSL.SP.2006.267.01.05

Tourloukis, V., and Harvati, K. (2018). The Palaeolithic Record of Greece: A Synthesis of the Evidence and a Research Agenda for the Future. *Quat. Int.* 466, 48–65. doi:10.1016/j.quaint.2017.04.020

Tourloukis, V., and Karkanas, P. (2012). The Middle Pleistocene Archaeological Record of Greece and the Role of the Aegean in Hominin Dispersals: New Data and Interpretations. *Quat. Sci. Rev.* 43, 1–15. doi:10.1016/j.quascirev.2012.04.004

Tourloukis, V., Muttoni, G., Karkanas, P., Monesi, E., Scardia, G., Panagopoulou, E., et al. (2018a). Magnetostratigraphic and Chronostratigraphic Constraints on the Marathousa 1 Lower Palaeolithic Site and the Middle Pleistocene Deposits of the Megalopolis Basin, Greece. *Quat. Int.* 497, 154–169. doi:10.1016/j.quaint.2018.03.043

Tourloukis, V. (2016). "On the Spatio-Temporal Distribution of Mediterranean Lower Paleolithic Sites: A Geoarchaeological Perspective," in *Paleoanthropology of the Balkans and Anatolia: Human Evolution and its Context. Vertebrate Paleobiology and Paleoanthropology Series*. Editors K. Harvati and M. Roksandic (Dordrecht: Springer-Verlag), 303–323. doi:10.1007/978-94-024-0874-4_18

Tourloukis, V., Thompson, N., Panagopoulou, E., Giusti, D., Konidaris, G. E., Karkanas, P., et al. (2018b). Lithic Artifacts and Bone Tools from the Lower Palaeolithic Site Marathousa 1, Megalopolis, Greece: Preliminary Results. *Quat. Int.* 497, 47–64. doi:10.1016/j.quaint.2018.05.043

Trauth, M. H. (2014). A New Probabilistic Technique to Build an Age Model for Complex Stratigraphic Sequences. *Quat. Geochronol.* 22, 65–71. doi:10.1016/j.quageo.2014.03.001

Trauth, M. H., Gebbers, R., Marwan, N., and Sillmann, E. (2015). *MATLAB Recipes for Earth Sciences*. 4th edition. doi:10.1007/978-3-662-46244-7

Tsiftsis, E. V. (1987). *Geology and Hydrogeology of the Megalopolis Basin, Peloponnese, Greece*. Doctoral dissertation, University of Bristol.

Tzedakis, P. C., Hooghiemstra, H., and Pälike, H. (2006). The Last 1.35 Million Years at Tenaghi Philippon: Revised Chronostratigraphy and Long-Term Vegetation Trends. *Quat. Sci. Rev.* 25 (23–24), 3416–3430. doi:10.1016/j.quascirev.2006.09.002

Unkel, I., Heymann, C., Nelle, O., and Zagana, E. (2011). "Climatic Influence on Lake Stymphalia during the Last 15 000 Years,". *Advances in the Research of Aquatic Environment*. Editor N. Lambrakis, G. Stournaras, and K. Katsanou (Berlin, Heidelberg: Springer), Vol. 1, 75–82. doi:10.1007/978-3-642-19902-810.1007/978-3-642-19902-8_8

Valero-Garcés, B., Morellón, M., Moreno, A., Corella, J. P., Martín-Puertas, C., Barreiro, F., et al. (2014). Lacustrine Carbonates of Iberian Karst Lakes: Sources, Processes and Depositional Environments. *Sediment. Geology* 299, 1–29. doi:10.1016/j.sedgeo.2013.10.007

Van Vugt, N., de Bruijn, H., van Kolfschoten, T., and Langereis, C. G. (2000). Magneto- and Cyclostratigraphy and Mammal-Fauna's of the Pleistocene Lacustrine Megalopolis Basin, Peloponnesos, Greece. *Geologica Ultrajectina* 189, 69–92.

Van Vugt, N., Langereis, C. G., and Hilgen, F. J. (2001). Orbital Forcing in Pliocene–Pleistocene Mediterranean Lacustrine Deposits. *Dominant Expr. eccentricity versus precession, Palaeogeogr. Palaeoclimatol. Palaeoecol.* 172 (3-4), 193–205. doi:10.1016/s0031-0182(01)00270-x

Varga, G., Újvári, G., and Kovács, J. (2014). Spatiotemporal Patterns of Saharan Dust Outbreaks in the Mediterranean Basin. *Aeolian Res.* 15, 151–160. doi:10.1016/j.aeolia.2014.06.005

Villa, V., Pereira, A., Chaussé, C., Nomade, S., Giaccio, B., Limondin-Lozouet, N., et al. (2016). A MIS 15-MIS 12 Record of Environmental Changes and Lower Palaeolithic Occupation from Valle Giumentina, central Italy. *Quat. Sci. Rev.* 151, 160–184. doi:10.1016/j.quascirev.2016.09.006

Vinken, R. (1965). Stratigraphie und Tektonik des Beckens von Megalopolis (Peloponnes, Griechenland). *Geologisches Jahrbuch* 83, 97–148.

Wagner, B., Vogel, H., Francke, A., Friedrich, T., Donders, T., Lacey, J. H., et al. (2019). Mediterranean winter Rainfall in Phase with African Monsoons during the Past 1.36 Million Years. *Nature* 573 (7773), 256–260. doi:10.1038/s41586-019-1529-0

Wagner, C. W. (1957). *Sur les ostracodes du Quaternaire récent de Pays Bas et leur utilization dans l'étude géologiques des dèpots Holocenes*. Mouton and Co. 'S-Gravenhage, 259.

Wang, P., Tian, J., and Lourens, L. J. (2010). Obscuring of Long Eccentricity Cyclicity in Pleistocene Oceanic Carbon Isotope Records. *Earth Planet. Sci. Lett.* 290 (3-4), 319–330. doi:10.1016/j.epsl.2009.12.028

Weiberg, E., Unkel, I., Kouli, K., Holmgren, K., Avramidis, P., Bonnier, A., et al. (2016). The Socio-Environmental History of the Peloponnese during the Holocene: Towards an Integrated Understanding of the Past. *Quat. Sci. Rev.* 136, 40–65. doi:10.1016/j.quascirev.2015.10.042

West, A., Galy, A., and Bickle, M. (2005). Tectonic and Climatic Controls on Silicate Weathering. *Earth Planet. Sci. Lett.* 235 (1-2), 211–228. doi:10.1016/j.epsl.2005.03.020

Williams, R. H., McGee, D., Kinsley, C. W., Ridley, D. A., Hu, S., Fedorov, A., et al. (2016). Glacial to Holocene Changes in Trans-Atlantic Saharan Dust Transport and Dust-Climate Feedbacks. *Sci. Adv.* 2 (11), e1600445. doi:10.1126/sciadv.1600445

Yaltirak, C., Sakinç, M., Aksu, A. E., Hiscott, R. N., Galleb, B., and Ulgen, U. B. (2002). Late Pleistocene Uplift History along the Southwestern Marmara Sea Determined from Raised Coastal Deposits and Global Sea-Level Variations. *Mar. Geology* 190 (1-2), 283–305. doi:10.1016/S0025-3227(02)00351-1

Conflict of Interest: The authors declare that the research was conducted in the absence of any commercial or financial relationships that could be construed as a potential conflict of interest.